

# New constraints on cosmic anisotropy from galaxy clusters using an improved dipole fitting method

Jianping Hu<sup>id, a</sup>, Chao Geng<sup>id, b</sup>, Xuandong Jia<sup>id, c</sup>, Zhaoyu Zuo<sup>id, a</sup>,  
Taozhi Yang<sup>id, a</sup> and Fayin Wang<sup>id, c,d</sup>

<sup>a</sup>Ministry of Education Key Laboratory for Nonequilibrium Synthesis and Modulation of Condensed Matter, School of Physics, Xi'an Jiaotong University, Xi'an 710049, China

<sup>b</sup>Department of Astronomy, University of Science and Technology of China, Hefei 230026, China

<sup>c</sup>School of Astronomy and Space Science, Nanjing University, Nanjing 210093, China

<sup>d</sup>Key Laboratory of Modern Astronomy and Astrophysics (Nanjing University), Ministry of Education, Nanjing 210093, China

E-mail: [hjp1206@163.com](mailto:hjp1206@163.com)

**Abstract.** The cosmological principle, as the cornerstone of the standard cosmological model, requires that the Universe be homogeneous and isotropic on a large scale. As one of its fundamental assumptions, it is constantly being tested by various types of data and methods. In this work, we attempted to apply the dipole fitting (DF) method to galaxy clusters to search for cosmic anisotropic signals, and to construct a statistical isotropic analysis scheme for them. Compared to Type Ia supernova (SNe Ia), the galaxy clusters offer a significant advantage in terms of spatial distribution. This advantage makes the anisotropic signals obtained from them more reliable. From 313 galaxy clusters (Chandra + XMM-Newton), we find two preferred directions  $(l, b) = (257.82^{\circ+58.01}_{-52.88}, -31.30^{\circ+35.92}_{-39.46})$  and  $(80.89^{\circ+60.97}_{-52.46}, 31.75^{\circ+35.19}_{-40.16})$ . The former to a direction where the universe is expanding at a faster rate than the surrounding area, while the latter to a slower rate of expansion. The corresponding magnitude of anisotropy is  $|A| = 5.2 \sim 5.4 \times 10^{-4}$ . The results of statistical isotropy analyses give  $\sim 1.0\sigma$  confidence level. From the reanalyses based on the subsamples including Chandra, XMM-Newton, low redshift (LR,  $z < 0.10$ ), high redshift (HR,  $z > 0.10$ ) datasets, we find that the observation equipment and sample redshift can affect the preferred direction, anisotropic magnitude, and statistical significance of anisotropy. The XMM-Newton dataset gives a statistical significance of  $2.26\sigma$  (Mock) and  $2.86\sigma$  (Iso) which are much higher than that from Chandra and the total datasets. The magnitude of anisotropy  $|A|$  from HR dataset is larger than that from LR dataset. Overall, our results indicate the presence of anisotropic signals in galaxy clusters, which must be taken seriously. Further test is still needed to better understand these signals.

---

## Contents

<b>1</b>	<b>Introduction</b>	<b>1</b>
<b>2</b>	<b>Data</b>	<b>3</b>
<b>3</b>	<b>Methodology</b>	<b>4</b>
3.1	X-ray luminosity-temperature relation	4
3.2	Dipole fitting method	5
3.3	Statistical isotropic analyses	6
<b>4</b>	<b>Results</b>	<b>6</b>
4.1	Constraints of the $L_X - T$ correlation	6
4.2	Anisotropic signal from different galaxy cluster samples	7
4.3	Anisotropic signal from different redshift subsamples	10
4.4	Statistical isotropic results	11
<b>5</b>	<b>Discussion</b>	<b>11</b>
<b>6</b>	<b>Summary</b>	<b>18</b>

---

## 1 Introduction

The  $\Lambda$  cold dark matter (CDM) model is widely recognized as the standard cosmological model, as it aligns well with the majority of astronomical observations [1–16]. Despite its remarkable success in explaining the majority of astronomical observations, this model is encountering increasing challenges as the volume and precision of observations continue to grow. In addition to the recent hot issues such as Hubble constant ( $H_0$ ) tension [17–24],  $S_8$  tension [25–29], dynamic dark energy [16, 30–33, 33–38], evolutionary behavior of  $H_0$  [39–46], there are also the growth tension [47–49], age of the universe [50, 51], Baryon Acoustic Oscillation (BAO) curiosities [52–54], small-scale curiosities [55, 56] and cosmic anisotropy [57–65]. Research related to the above topics indicates that the  $\Lambda$ CDM model might have limitations in describing the structure and evolution of the Universe. Thus, its status as the standard cosmological model remains contingent upon validation through more precise astronomical observations [66, 67].

Cosmological principle, as the basic assumption of the  $\Lambda$ CDM model, requires that the universe is statistically isotropic and uniform on a sufficiently large scales. Due to the high significance of this hypothesis, it is necessary that it is robustly scrutinized and tested against different cosmological probes using the latest data samples [68]. Numerous studies suggest that the Universe might be inhomogeneous and anisotropic; such as the cosmic microwave background (CMB) [69–74], fine-structure constant [75–77], direct measurement of the Hubble parameter [78], anisotropic dark energy [79–81], anisotropic matter density [82], anisotropic Hubble constant [83, 84], large dipole of radio source counts [85–87], and so on. These studies are based on different types of observations, including galaxies [88–91], galaxy spin direction [92], galaxy cluster [68, 93–97], dwarf galaxies [98], quasar [99–104, 104–108], CosmicFlows-4 [109], gamma-ray burst [GRB; 110–112], type Ia supernovae

[SNe Ia; 113–120] and their joint datasets [121–125]. Recently, some researches have shown that the local cosmic anisotropy might significantly affect the local constraints on  $H_0$  [126–128]. The evolution behavior of  $H_0$  and the Hubble tension might be closely related to the violation of cosmological principle in the local universe [129, 130]. Therefore, precise testing of the cosmological principle can not only help us better understand the current state of the Universe, but also aid in exploring the physical origin of the  $H_0$  evolutionary behavior and the Hubble tension.

Currently, type Ia supernovae are the most commonly used late-time cosmological probe to test the cosmological principle [121, 129, 131–141]. Its combination with the hemispheric comparison method [137, 142, 143], dipole fitting method [75, 128, 144], and regional fitting method [129] can well reflect the anisotropy level of the local universe. SNe Ia observations reveal departures from isotropy at confidence levels from 1.4 to  $4.7\sigma$  [120, 121, 129, 135, 137, 145]. It is worth to note that the latest Pantheon+ SNe Ia are still not uniformly distributed in the sky; some SNe are very concentrated, forming a belt-like structure that is the SDSS sample [146]. A large number of researches have explored the impact of inhomogeneous distribution of SNe on the results of cosmic anisotropy, and found that the unevenness of the spatial distribution of samples will affect the preferred direction of anisotropy [147, 148] and contribute a certain level of anisotropy [129, 137]. To circumvent this problem, on the one hand, a subsample with uniform spatial distribution can be selected from the existing observations. On the other hand, the influence of the band structure can be weakened by adding new measurements. Of course, the most straightforward approach is to utilize other type of uniformly distributed observations, such as quasars [149–151] and galaxy clusters [68, 152]. Therefore, the development of other new uniformly distributed probes that can be used to test the cosmological principle should be encouraged. Not long ago, Migkas et al. [68] compiled a new sample of galaxy clusters consisting of 313 homogeneously selected sources from the Meta-Catalogue of X-ray detected Clusters of galaxies. Combining the sky scanning method, they found a strong anisotropy toward Galactic coordinates ( $280^\circ$ ,  $-20^\circ$ ) with  $\geq 4.0\sigma$  confidence level. Until now, no research has considered utilizing the dipole fitting (DF) method to probe the cosmological principle from the galaxy cluster observations. Furthermore, there is currently no statistical isotropic analysis scheme applicable to the DF method.

In this study, we combined the DF method with galaxy cluster observation for the first time to test the cosmological principle, and construct a statistical isotropic analysis scheme for them. Our goal is to probe anisotropic signals from galaxy clusters, assess the statistical significance of anisotropy, and analyze the potential impact of factors such as data spatial distribution, observation equipment, and redshift on the probed results. The paper is organized as follows: In Section 2 we briefly introduce the basic information of the galaxy cluster sample used and give its redshift distribution and spatial location distribution. Section 3 details how to combine the  $L_X - T$  relation of galaxy clusters with the DF method to probe the preferred direction of cosmic anisotropy. It also describes how to construct statistical isotropic analyses to evaluate the significance of the results. In Section 4, we present the main results, including the constraints of  $L_X - T$  correlation, the anisotropic signals derived from various galaxy cluster datasets, and the corresponding statistical results. Afterwards, the corresponding investigation and discussion are given in Section 5. Finally, a brief summary is given in Section 6.

## 2 Data

Galaxy cluster sample used in this work was screened by Migkas et al. [68] from the Meta-Catalogue as of July 2019 of X-ray detected Clusters of galaxies [MCXC; 152]. The parent catalogs of the clusters consists of the ROSAT extended Brightest Cluster Sample [eBCS; 153], the Northern ROSAT All-Sky (NORAS) Galaxy Cluster Survey [154] and the ROSAT-ESO Flux-Limited X-Ray (REFLEX) Galaxy Cluster Survey Catalog [155]. They are all based on the ROSAT All-Sky Survey [RASS; 156]. The basic selection criteria are that these clusters have high-quality Chandra [157] or XMM-Newton [158] public observations. More detailed screening conditions can be found from the section 2 in [68].

The total sample used in this paper comprises 313 galaxy clusters, spanning a redshift range of 0.004 to 0.447. This sample is derived from two datasets: Chandra and XMM-Newton. The former contains 237 clusters with a redshift range of (0.004, 0.447). The latter contains 76 clusters with a redshift range of (0.018, 0.244). By comparing the redshift range, it can be find that compared with the XMM-Newton dataset, the Chandra dataset cover a wider redshift range and have more high-redshift observations. We gave the redshift distributions of different types datasets in the left panel of figure 1. It can help us better understand the composition structure and redshift distribution of the datasets used. From the redshift distribution of the total sample, it is easy to find most of the observed redshifts are less than 0.10. For convenience, we refer to the dataset with redshift below 0.10 as LR dataset. It consists of 219 clusters accounting for about 70% of the total sample. It is mainly contributed by the Chandra observation (162 clusters) and a small part by the XMM-Newton observation (57 clusters). There are 94 clusters with redshift greater than 0.10, including 75 Chandra measurements and 19 XMM-Newton measurements. This sample is called the HR dataset. Meanwhile, we also mapped their location distributions in the galactic coordinate system, as shown in the right panel of figure 1. Compared to SNe Ia, the spatial distribution of galaxy cluster is more uniform. In the SNe Ia samples (for example Pantheon and Pantheon+), there is a data-rich band structure [4], which significantly affect the overall uniformity of the observations [129, 137]. From the comparison of Chandra and XMM-Newton datasets, we find that the Chandra observation is more uniform than the XMM-Newton observation in terms of spatial distribution. Overall, the spatial distribution of galaxy clusters is relatively uniform, making them suitable for testing the cosmological principle.

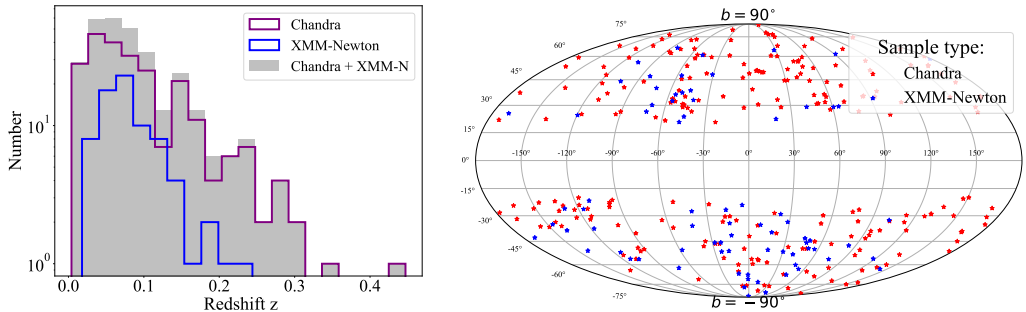


**Figure 1.** Basic information of the galaxy cluster dataset. Redshift distribution (left panel) and location distribution (right panel) in the galactic coordinate system.

### 3 Methodology

#### 3.1 X-ray luminosity-temperature relation

It is well-known that galaxy clusters are the most massive gravitationally bound systems in the Universe, strongly emitting X-ray photons due to the large amounts of hot gas they contain ( $\sim 10\%$  of their total mass) in their intra-cluster medium (ICM). Their physical quantities follow tight scaling relations, for which Kaiser [159] provided mathematical expressions. Specifically, the correlation between the X-ray luminosity ( $L_X$ ) and the ICM gas temperature ( $T$ ) of galaxy clusters is of particular interest since it can be used to test the cosmological principle.

The general properties of the  $L_X - T$  scaling relation have been extensively scrutinized in the past by several authors [68, 93, 94, 160–170]. A standard power-law form of the  $L_X - T$  relation are as follows [163]:

$$\frac{L_X}{10^{44}\text{erg/s}} E(z)^{-1} = k \times \left(\frac{T}{4\text{keV}}\right)^s, \quad (3.1)$$

where term  $E(z) = \sqrt{\Omega_m(1+z)^3 + \Omega_\Lambda}$  scales  $L_X$  accordingly to explain the redshift evolution of the  $L_X - T$  relation. Parameters  $k$  and  $s$  are the free parameters to be fitted. Parameters  $L_X$  and  $T$  represent the X-ray luminosity and temperature, respectively.  $L_X$  is strongly related to cosmology, and can be derived from the formula  $L_X = 4\pi d_L^2 F_0$ . Here,  $F_0$  represents the k-corrected flux, and  $d_L$  represents the luminosity distance. Considering a spatially flat  $\Lambda$ CDM model, the luminosity distance  $d_L$  can be derived from the following formal

$$d_L = \frac{c(1+z)}{H_0} \int_0^z \frac{dz'}{\sqrt{\Omega_m(1+z')^3 + \Omega_\Lambda}}, \quad (3.2)$$

where  $c$  is the speed of light,  $H_0$  is the Hubble constant,  $\Omega_m$  and  $\Omega_\Lambda$  are the matter parameter and the dark energy (DE) parameter respectively, satisfying  $\Omega_m + \Omega_\Lambda = 1$ . Equation (3.1) can be written in logarithmic form as follows:

$$\log \mathcal{L}_X = \log k + s \log \mathcal{T}, \quad (3.3)$$

where

$$\mathcal{L}_X = \frac{L_X}{10^{44}\text{erg/s}} E(z)^{-1} \quad \text{and} \quad \mathcal{T} = \frac{T}{4\text{keV}}. \quad (3.4)$$

Constraints on the free parameters of  $L_X - T$  relation to be fitted can be derived by minimizing corresponding  $\chi^2_{\text{Cluster}}$ ,

$$\chi^2_{\text{Cluster}} = \sum_{i=1}^N \frac{\log [\mathcal{L}_{X,obs}] - \log [\mathcal{L}_{X,th}(\mathcal{T}, P_n)]}{\sigma_{\log L_i}^2 + s^2 \times \sigma_{\log T_i}^2 + \sigma_{int}^2}, \quad (3.5)$$

where  $N$  represents the number of clusters used in analyzing,  $\mathcal{L}_{X,th}$  is the theoretical X-ray luminosity based on the measured temperature  $T$ , and  $P_n$  represents the parameters ( $H_0$ ,  $\Omega_m$ ,  $k$ ,  $s$ , and  $\sigma_{int}$ ) to be fitted.  $\mathcal{L}_{X,obs}$  is the observed X-ray luminosity which derived by the observed flux based on a fix cosmological model. Furthermore,  $\sigma_{\log L_i}$  and  $\sigma_{\log T_i}$  are the corresponding  $1\sigma$  errors.  $\sigma_{int}$  is the intrinsic scatter of the  $L_X - T$  correlation, which is

usually used to describe the compactness of the correlation; the smaller the value, the more compact the relationship. More information on the  $L_X - T$  relation and its cosmological applications can be found from the review article [96].

It is worth noting that the cosmological parameters and the  $L_X - T$  correlation parameters cannot be constrained simultaneously since they are degenerate. Therefore, one needs to fix one of the parameters to investigate the behavior of the other. In this paper, the observed X-ray luminosity  $\mathcal{L}_{X,obs}$  is derived utilizing  $L_X$  which provided by [68]. They calculated  $L_X$  based on the flat  $\Lambda$ CDM cosmology with  $\Omega_m = 0.30$ ,  $\Omega_\Lambda = 0.70$ , and  $H_0 = 70.0$  km/s/Mpc.

### 3.2 Dipole fitting method

Dipole fitting (DF) method was proposed to find the fine structure constant  $(\Delta\alpha/\alpha)$  dipole [75]. This approach constructs a dipole+monopole model which constitutes the first two term of the spherical harmonic expansion. Instead of  $(\Delta\alpha/\alpha)$ , which corresponds to fine structure constant deviations from its earth measured value, Mariano & Perivolaropoulos [79] first applied this method to probe the dark energy dipole based on the distance modulus  $\mu$ . The basic equation is as follows

$$\left(\frac{\Delta\mu(z)}{\mu(z)_{th}}\right) \equiv \frac{\mu(z)_{obs} - \mu(z)_{th}}{\mu(z)_{th}} = A \cos \theta + B, \quad (3.6)$$

where  $\cos \theta$  is the angle with the dipole axis,  $A$  is the dipole magnitude, and  $B$  is the monopole magnitude. Afterwards, it was widely used to probe the preferred direction of cosmic anisotropy [128, 171, 172]. In this paper, we applied this method for galaxy clusters for the first time to test the cosmological principle. In order to make the DF method applicable to galaxy cluster, we used  $(\Delta \log L_X / \log L_X)$  instead of  $(\Delta\alpha/\alpha)$ , and the modified form is as follows:

$$\left(\frac{\Delta \log L_X}{\log L_{X,th}(z)}\right) \equiv \frac{\log L_{X,obs}(z) - \log L_{X,th}(z)}{\log L_{X,th}(z)} = A \cos \theta + B. \quad (3.7)$$

Then, we can simplify eq. (3.7) to the following form

$$\log \tilde{L}_{X,th} = \log L_{X,th} \times (1 + A \cos \theta + B), \quad (3.8)$$

where  $\log \tilde{L}_{X,th}$  represents the modified theoretical X-ray luminosity. The angle with the dipole axis,  $\cos \theta$ , is defined by

$$\cos \theta = \hat{\mathbf{n}} \cdot \hat{\mathbf{p}}, \quad (3.9)$$

here,  $\hat{\mathbf{n}}$  and  $\hat{\mathbf{p}}$  correspond to the dipole direction and the unit vector pointing to the position of galaxy clusters, respectively. In the galactic coordinate, the form of  $\hat{\mathbf{n}}$  can be written as

$$\hat{\mathbf{n}} = \cos(b) \cos(l) \hat{\mathbf{i}} + \cos(b) \sin(l) \hat{\mathbf{j}} + \sin(b) \hat{\mathbf{k}}. \quad (3.10)$$

For any observational source whose location is  $(l_i, b_i)$ ,  $\hat{\mathbf{p}}$  is given by

$$\hat{\mathbf{p}}_i = \cos(b_i) \cos(l_i) \hat{\mathbf{i}} + \cos(b_i) \sin(l_i) \hat{\mathbf{j}} + \sin(b_i) \hat{\mathbf{k}}. \quad (3.11)$$

Substituting eqs. (3.8) into (3.3), we can derive the modified form of  $\log \mathcal{L}_X$ ; that is,  $\log \tilde{\mathcal{L}}_{X,th}$ . Substitute  $\log \tilde{\mathcal{L}}_{X,th}$  into eq. (3.5), we can obtain a new chi-square function ( $\chi^2_{\text{Cluster,DF}}$ ), which takes into account the dipole-monopole correction and has the following form:

$$\chi^2_{\text{Cluster,DF}} = \sum_{i=1}^N \frac{\log [\mathcal{L}_{X,obs}] - \log [\tilde{\mathcal{L}}_{X,th}(\mathcal{T}, P_n)]}{\sigma_{\log L_i}^2 + s^2 \times \sigma_{\log T_i}^2 + \sigma_{int}^2}. \quad (3.12)$$

There are total 7 parameters to be fitted, including the correlation parameters ( $k$ ,  $s$  and  $\sigma_{int}$ ) and the correction parameters ( $l$ ,  $b$ ,  $A$  and  $B$ ). The coordinate ( $l$ ,  $b$ ) represents the preferred direction (longitude, latitude) in the galactic coordinate system. The parameters  $A$  and  $B$  are used to describe the level of anisotropy.

If the galaxy cluster observations are more favorable to an isotropic universe, the values of  $A$  and  $B$  will be closer to zero. The non-zero  $A$  or  $B$  indicate that the observations favor an anisotropic universe. In general, the DF method can yield two sets of constraints; that is two preferred directions of cosmic anisotropy. These two preferred directions are almost symmetric in the galactic coordinate system, and have mutually negative  $A$  values and similar  $B$  values. In the direction corresponding to the positive  $A$  value, the universe is expanding faster than the surrounding, while in the direction corresponding to negative  $A$  values, the universe expands slower than its surroundings. For the parameter  $B$ , a positive value means that the universe is expanding slower than expected by the  $\Lambda$ CDM model. For the galaxy cluster, a positive  $A$  indicates that at the same redshift, the source in the preferred direction is brighter. The positive  $B$  values indicate the observation is brighter overall. Otherwise, the corresponding results are the opposite.

### 3.3 Statistical isotropic analyses

In order to examine whether the dipole magnitude  $A$  obtained from the galaxy cluster sample are consistent with isotropy, we plan to perform statistical isotropy analyses. Here, we construct a statistical isotropic analysis for the dipole fitting method for the first time. First, we need to fix parameters  $l$  and  $b$  based on the constraints of the preferred direction from the real data. The  $A$  values corresponding to the two preferred directions are negative of each other, and their absolute values are similar. Therefore, fixing any direction has little impact on the statistical results. Here, we choose the direction ( $l$ ,  $b$ ) corresponding to the negative  $A$  value, as the expansion rate in this direction is faster than the surrounding areas. Then, we use simulated data to constraint parameters  $A$  and  $B$ . Parameter  $A$  is used to evaluate the statistical significance of the real data. In the statistical analyses, we considered two schemes: one is to preserve the spatial coordinates of the real data and then randomly place the galaxy clusters. For convenience, we refer this scheme as "Mock". After that, we can obtain the constraints of the correction parameters ( $A$  and  $B$ ) for the simulated datasets. If the non-uniform distribution of the observations can affect the results, the constraints of  $A$  obtained from simulated datasets will deviate from zero. As a comparison, we also considered another scheme, that is removing the location information and evenly distributing the real data across the celestial sphere. For convenience, we refer this scheme as "Iso". By comparing the  $A$  values obtained from the two schemes, the degree of influence of spatial distribution on the results can be estimated. Considering the limitations of computation time, we generated 1000 sets of simulation data; this yielded acceptable statistics.

## 4 Results

### 4.1 Constraints of the $L_X - T$ correlation

First, we gave the constraints of  $L_X - T$  correlation using the different galaxy cluster datasets, including Chandra, XMM-Newton and Chandra + XMM-Newton. For the Chandra dataset, the best fitting results are  $k = 1.15 \pm 0.05$ ,  $s = 2.14 \pm 0.06$  and  $\sigma_{int} = 0.24 \pm 0.01$ . For the XMM-Newton dataset, the best fitting results are  $k = 0.99_{-0.07}^{+0.06}$ ,  $s = 1.53 \pm 0.14$  and  $\sigma_{int} = 0.23_{-0.03}^{+0.02}$ . For the total sample (Chandra + XMM-Newton), the corresponding results are  $k$

$= 1.12 \pm 0.04$ ,  $s = 2.07 \pm 0.06$  and  $\sigma_{int} = 0.24 \pm 0.01$ . The corresponding  $L_X - T$  diagrams and confidence contours are displayed in figure 2.

Afterwards, we also gave the constraints in different redshift intervals. The total sample is divided into two sub-samples according to redshift: low redshift subsample (LR; redshift  $\leq 0.10$ ) and high redshift subsample (HR; redshift  $> 0.10$ ). For the LR dataset, the best fits are  $k = 1.01 \pm 0.04$ ,  $s = 1.92 \pm 0.08$  and  $\sigma_{int} = 0.26^{+0.01}_{-0.02}$ . For the HR dataset, the corresponding results are  $k = 1.89^{+0.15}_{-0.18}$ ,  $s = 1.57 \pm 0.13$  and  $\sigma_{int} = 0.17^{+0.01}_{-0.02}$ . The corresponding  $L_X - T$  diagrams and confidence contours are showed in figure 3. All numerical results are summary in table 1. According to the constraints of the  $L_X - T$  relation, we can use galaxy clusters to test cosmological principle and search for the preferred direction of cosmic anisotropy.

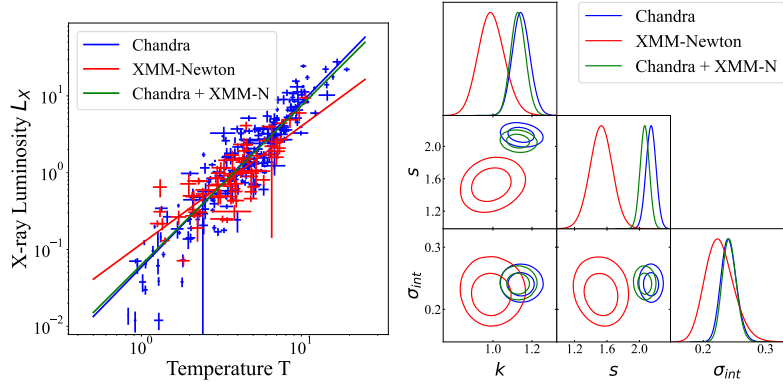


**Figure 2.**  $L_X - T$  diagrams (left panel) and the corresponding confidence contours (right panel) for different types datasets. Blue, red and green represent the results from Chandra, XMM-Newton, and Chandra + XMM-Newton datasets, respectively.

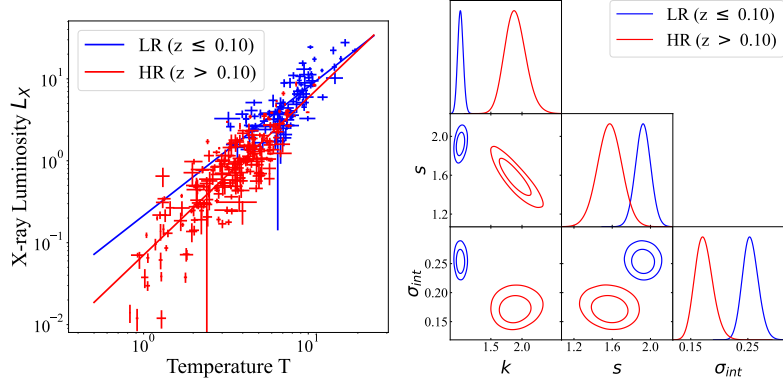


**Figure 3.**  $L_X - T$  diagrams (left panel) and the corresponding confidence contours (right panel) for different redshift datasets. Blue and red represent the results from LR and HR datasets, respectively.

## 4.2 Anisotropic signal from different galaxy cluster samples

We applied the DF method to the galaxy cluster to search for the preferred direction of the cosmic anisotropy. From the description of the DF method in Sect. 3.2, we can see that there are a total of 7 free parameters: correlation parameters ( $k$ ,  $s$  and  $\sigma_{int}$ ), and correction parameters ( $l$ ,  $b$ ,  $A$  and  $B$ ). In order to obtain more accurate constraints on the preferred

**Table 1.** Constraints of the  $L_X - T$  correlation ( $k$ ,  $s$ , and  $\sigma_{int}$ ) from different galaxy cluster datasets.

Sample	$k$	$s$	$\sigma_{int}$
Chandra	$1.15 \pm 0.05$	$2.14 \pm 0.06$	$0.24 \pm 0.01$
XMM-Newton	$0.99^{+0.06}_{-0.07}$	$1.53 \pm 0.14$	$0.23^{+0.02}_{-0.03}$
Chandra + XMM-N	$1.12 \pm 0.04$	$2.07 \pm 0.06$	$0.24 \pm 0.01$
LR ( $z \leq 0.10$ )	$1.01 \pm 0.04$	$1.92 \pm 0.08$	$0.26^{+0.01}_{-0.02}$
HR ( $z > 0.10$ )	$1.89^{+0.15}_{-0.18}$	$1.57 \pm 0.13$	$0.17^{+0.01}_{-0.02}$

direction  $(l, b)$ , it is better to fix the correlation parameters ( $k$ ,  $s$  and  $\sigma_{int}$ ). Thus, we fixed the correlation parameters according to the constraints of  $L_X - T$  relation in Section 4.1 to search for cosmic anisotropic signals.

The constraints of correction parameters obtained from different types datasets (Chandra + XMM-N, Chandra, and XMM-Newton) are displayed in figure 4. As expected, two best fits (two peaks) for parameters  $l$ ,  $b$ , and  $A$  are obtained. In other words, there are two preferred directions  $(l, b)$ . The positive  $A$  value corresponds to a direction in which the universe expands slower than the surroundings, and the negative  $A$  value corresponds to a direction in which the universe expands faster than the surroundings. These two directions are almost symmetrical in the galactic coordinate system. Here, we need to emphasize that if the two best fit values are very close to zero, it will make the result look like there is only one best fit value, zero. This phenomenon is particularly prominent in the constraints of parameter  $A$  [128]. Based on the confidence contours in figure 4, by narrowing the prior range of the parameter  $l$ , we can separate the constraints in a single direction  $(l, b)$  and their corresponding correction parameters ( $A$  and  $B$ ). This means that we perform two separate constraints, resulting in two sets of constraints. We put the two sampling results of parameter  $A$  on the same canvas to help us better understand the unimodal constraints of parameter  $A$  in figure 4, as shown in figure 5.

For the Chandra + XMM-N dataset, the two preferred directions  $(l, b)$  are

$$(l, b) = (257.82^\circ_{-52.88}^{+58.01}, -31.30^\circ_{-39.46}^{+35.92})$$

and

$$(l, b) = (80.89^\circ_{-52.46}^{+60.97}, 31.75^\circ_{-40.16}^{+35.19}),$$

respectively. The corresponding constraints of correction parameters are

$$A = -5.4 \pm 6.3 \times 10^{-4}, \quad B = 0.5 \pm 3.2 \times 10^{-4},$$

and

$$A = 5.2^{+6.5}_{-5.8} \times 10^{-4}, \quad B = 0.4 \pm 3.2 \times 10^{-4}.$$

For the Chandra dataset, two sets of constraints are

$$l = 328.31^\circ_{-63.56}^{+66.52}, \quad b = -2.91^\circ_{-52.27}^{+57.78},$$

$$A = -1.9^{+6.8}_{-6.2} \times 10^{-4}, \quad B = -0.6 \pm 3.7 \times 10^{-4},$$

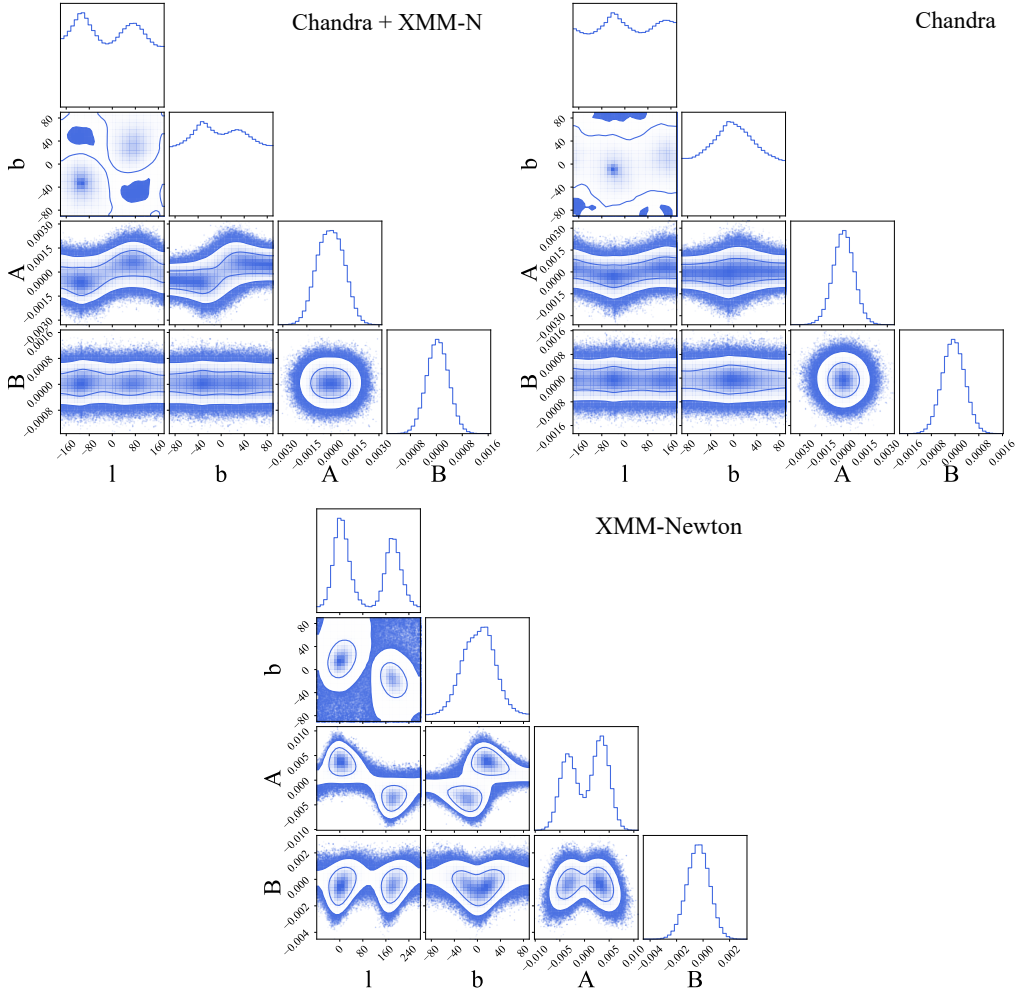


**Figure 4.** Confidence contours ( $1\sigma$  and  $2\sigma$ ) of the correction parameters ( $l$ ,  $b$ ,  $A$ , and  $B$ ) for different types datasets, including Chandra + XMM-N, Chandra and XMM-Newton.

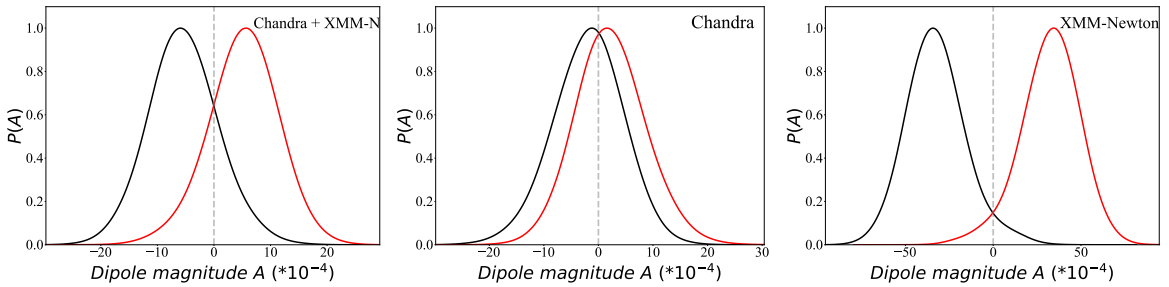


**Figure 5.** Constraints of dipole magnitude  $A$  of different types datasets, including Chandra + XMM-N, Chandra and XMM-Newton. .

and

$$l = 148.32^{\circ+60.16}_{-57.50}, \quad b = 4.62^{\circ+51.70}_{-57.03}, \\ A = 2.2^{+6.1}_{-6.8} \times 10^{-4}, \quad B = -0.6 \pm 3.7 \times 10^{-4},$$

respectively. For the XMM-Newton dataset, the corresponding results are

$$l = 184.42^{\circ+29.01}_{-24.58}, \quad b = -17.73^{\circ+18.55}_{-21.53}, \\ A = -32.0^{\pm 15.0}_{-18.0} \times 10^{-4}, \quad B = -3.9 \pm 8.1 \times 10^{-4},$$

and

$$l = 5.0^{\circ+28.81}_{-25.33}, \quad b = 17.61^{\circ+21.56}_{-18.68}, \\ A = 32.0^{\pm 18.0}_{-15.0} \times 10^{-4}, \quad B = -3.9 \pm 8.0 \times 10^{-4}.$$

The numerical results are placed in table 2. In addition to considering the effects of datasets on the results, we also investigated the impact of redshift on the anisotropic signal, and the results are described in the next section.

### 4.3 Anisotropic signal from different redshift subsamples

In order to fully discuss the factors that might have influenced the anisotropic signal, we divide the total sample into two subsamples based on the redshift value of 0.10 to investigate the effect of redshift on the results. According to the constraints of the  $L_X - T$  correlation in Section 4.1, we fixed the parameters  $k$ ,  $s$  and  $\sigma_{int}$ , and then to constrain the preferred direction ( $l$ ,  $b$ ) as well as the dipole-monopole correction parameters  $A$  and  $B$ . The final constraints are shown in figure 6. By narrowing the prior range of the parameter  $l$ , we can obtain the constraints of each preferred direction and its corresponding correction parameters. Meanwhile, we also put the two sampling results of parameter  $A$  on the same canvas to help understand the probability density distribution of  $A$  in figure 6, as shown in figure 7.

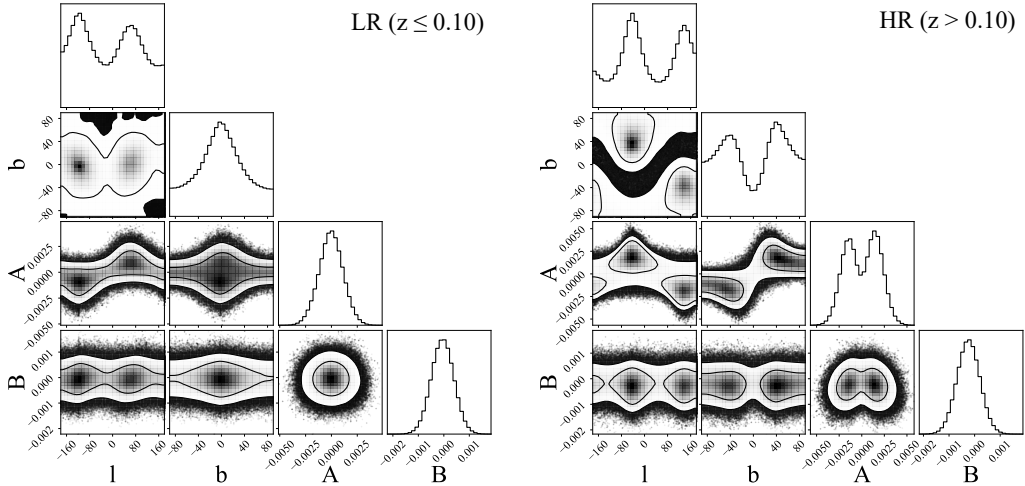


**Figure 6.** Confidence contours ( $1\sigma$  and  $2\sigma$ ) of the correction parameters ( $l$ ,  $b$ ,  $A$ , and  $B$ ) for different redshift datasets (LR and HR).

For the LR dataset, the corresponding results are as follow:

$$l = 247.66^{\circ+58.30}_{-49.20}, \quad b = -1.93^{\circ+45.43}_{-43.45}, \\ A = -6.5^{\pm 9.7}_{-8.0} \times 10^{-4}, \quad B = -0.9 \pm 4.2 \times 10^{-4},$$

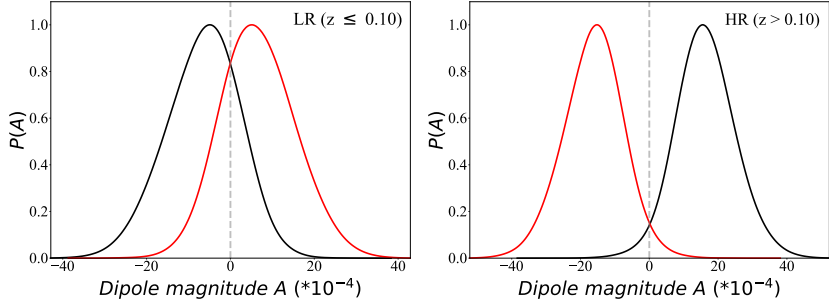


**Figure 7.** Constraints of dipole magnitude  $A$  of different redshift datasets (LR and HR).

and

$$l = 73.01^{\circ+62.39}_{-46.50}, \quad b = 2.21^{\circ+42.77}_{-44.55}, \\ A = 6.6^{+8.3}_{-9.6} \times 10^{-4}, \quad B = -0.8 \pm 4.2 \times 10^{-4}.$$

For the HR dataset, the two sets of constraints are

$$l = 139.84^{\circ+39.62}_{-35.47}, \quad b = -43.07^{\circ+21.52}_{-25.53}, \\ A = -16.2^{+9.0}_{-8.1} \times 10^{-4}, \quad B = -2.6 \pm 4.2 \times 10^{-4},$$

and

$$l = 320.57^{\circ+40.04}_{-35.15}, \quad b = 43.90^{\circ+25.52}_{-21.64}, \\ A = 16.3 \pm 8.8 \times 10^{-4}, \quad B = -2.5 \pm 4.3 \times 10^{-4}.$$

All numerical results are summarized in table 2.

#### 4.4 Statistical isotropic results

According to two schemes, utilizing 1000 simulated datasets, we performed statistical isotropic analyses for the different datasets. For the dipole correction, all statistical results ( $A_{\text{mock}}$ ) can be described by a Gaussian function. According to the statistical isotropic results, we can derive the statistical significances of the real data. For the Mock scheme, the statistical significance ( $D$ ) of the Chandra, XMM-Newton, and Chandra + XMM-Newton datasets are  $0.20\sigma$ ,  $2.26\sigma$ , and  $0.93\sigma$ , respectively. For the LR and HR datasets, the corresponding statistical significances are  $0.71\sigma$  and  $1.97\sigma$ , respectively. The statistical results of the Mock scheme are shown in figure 8. For the Iso scheme, the statistical significance has improved slightly. The statistical significance of the Chandra, XMM-Newton, and Chandra + XMM-Newton datasets are  $0.30\sigma$ ,  $2.86\sigma$ , and  $1.46\sigma$ , respectively. The statistical significance of the LR and HR datasets are  $0.87\sigma$  and  $2.31\sigma$ , respectively. The statistical results of the Iso scheme are shown in figure 9. Corresponding eigenvalues (expectation  $\mu$ , standard deviation  $\sigma$  and statistical significance  $D$ ) for these two schemes are collected in table 3.

## 5 Discussion

Before utilizing the galaxy clusters to explore the preferred direction of cosmic anisotropy, we need to constrain the  $L_X - T$  correlation for the different datasets, as shown in figure 2.

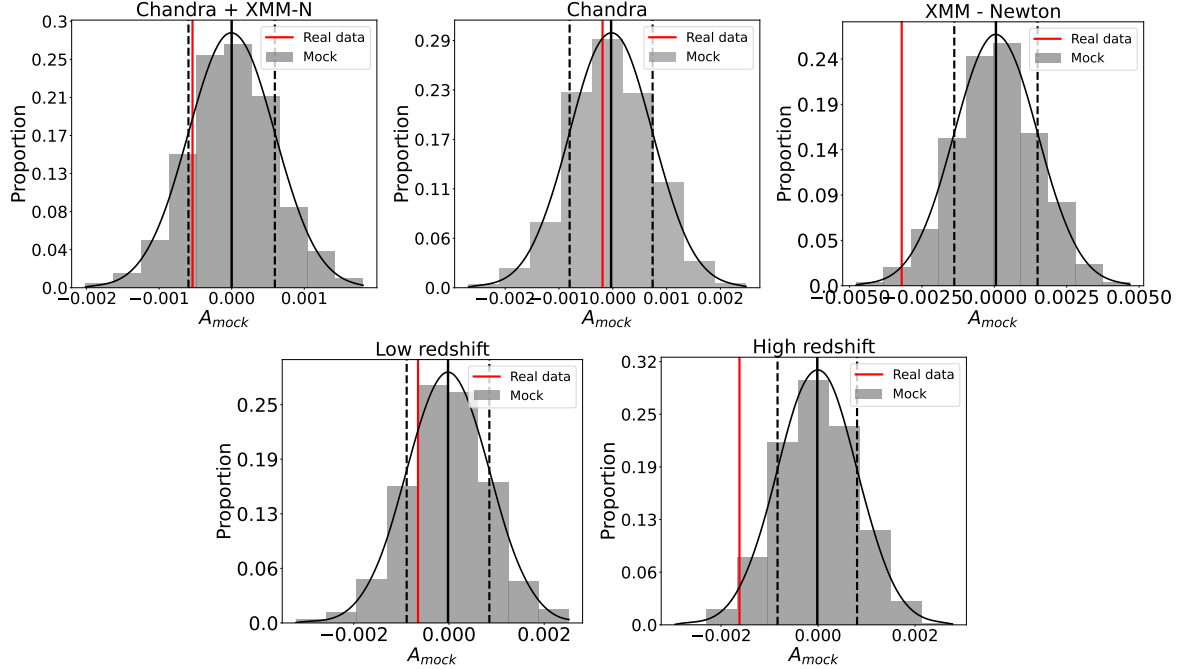


**Figure 8.** Statistical results in Mock scheme. The black curve is the best fit to the Gaussian function. The solid black and vertical dashed lines are commensurate with the mean and the standard deviation, respectively. The red lines represent the result of real data. The statistical significance ( $D$ ) of the Chandra, XMM-Newton, Chandra + XMM-Newton, LR and HR datasets are  $0.20\sigma$ ,  $2.26\sigma$ ,  $0.93\sigma$ ,  $0.71\sigma$  and  $1.97\sigma$ , respectively.

By comparing the constraints of  $L_X - T$  correlation from different datasets, we can find that there are obvious discrepancies between the constraints of  $L_X - T$  correlation obtained from the Chandra and the XMM-Newton datasets. The difference of parameter  $k$  is not obvious, only  $1.86\sigma$ , while the difference of parameter  $s$  is more obvious, reaching  $4.01\sigma$ . The reasons for this discrepancy are currently unclear and require further study. The ones of total sample (Chandra + XMM-Newton) are more inclined to Chandra's results. At the same time, we also gave the constraints of  $L_X - T$  correlation from different redshift subsamples, including LR ( $z < 0.10$ ) and HR ( $z > 0.10$ ), as shown in figure 3. Obviously, the parameter  $k$  from LR dataset is closer to that of the XMM-Newton dataset. This result is somewhat beyond our expectations. Intuitively, the Chandra dataset dominates the LR dataset, accounting for about 75%. The results should be more inclined to Chandra's results. For the HR dataset, the parameter  $k$  is significantly different from the LR results. For parameter  $k$ , the discrepancy  $\Delta k$  is 0.88, with a significance of  $5.18\sigma$ . For parameter  $s$ , the difference is not significant, with a difference of 0.35 and a significance of  $2.29\sigma$ . These findings suggest that the  $L_X - T$  correlation might evolve with redshift. This needs further study. Afterwards, we used these five galaxy cluster datasets with the DF method for exploring the preferred direction of cosmic anisotropy.

Based on the results of the  $L_X - T$  correlation, we fixed the  $L_X - T$  relationship parameters ( $k$ ,  $s$  and  $\sigma_{int}$ ), and then constrained the correction parameters ( $l$ ,  $b$ ,  $A$  and  $B$ ), as shown in figures 4 and 6. By comparing negative values of  $A$  and their corresponding preferred directions ( $l$ ,  $b$ ), we find significant differences between the degree of anisotropy and the preferred directions for the Chandra and XMM-Newton datasets. The latter gives

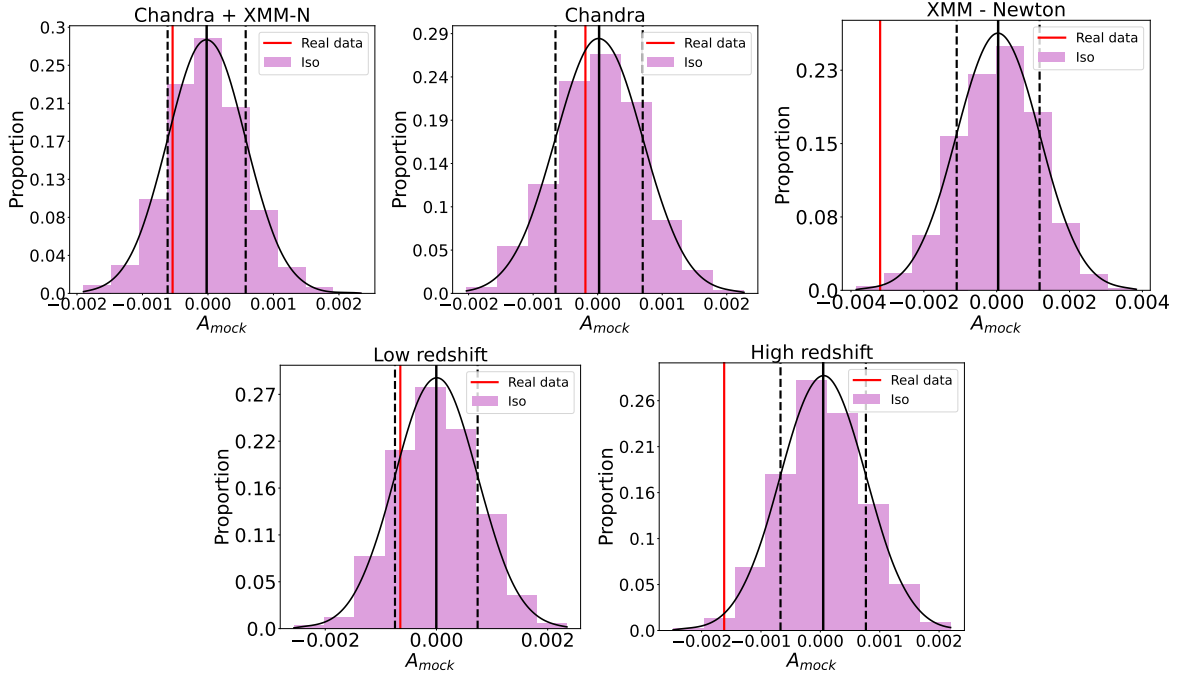


**Figure 9.** Statistical results in the Iso scheme. The black curve is the best fit to the Gaussian function. The solid black and vertical dashed lines are commensurate with the mean and the standard deviation, respectively. The red lines represent the result of real data. The statistical significance ( $D$ ) of the Chandra, XMM-Newton, Chandra + XMM-Newton, LR and HR datasets are  $0.30\sigma$ ,  $2.86\sigma$ ,  $0.91\sigma$ ,  $0.87\sigma$  and  $2.31\sigma$ , respectively.

stronger anisotropy (larger values of  $|A|$ ) and better constrains the preferred directions. For the anisotropic degree  $|A|$ , the difference between these two datasets is  $3.01 \times 10^{-3}$ , with the XMM-Newton dataset giving a stronger anisotropy signal. Combined with figure 5, it is easier for us to understand the difference in the degree of anisotropy. The further the best fit value deviates from zero, the stronger the anisotropy found. For the preferred direction, the difference in longitude between the two preferred directions is much greater than that in latitude, with a difference of  $143.89^\circ$ . Such stark discrepancies might be due to the evolution of the cosmic structure with redshift. Compared to Chandra dataset, the XMM-N dataset contains more high-redshift observations, as we mentioned in Section 2. This can be seen directly from the redshift distribution (left panel) in figure 1. The discrepancies might also be affected by the spatial distribution of observations. The Chandra dataset are better than the XMM-Newton dataset in terms of spatial distribution uniformity. This can be clearly seen from the right panel of figure 1. Furthermore, we could not rule out the influence of differences in observation equipment or unknown factors introduced during data processing. At present, it is impossible to determine the source of the discrepancies. Further analysis with more high-quality observations is needed to determine the physical mechanism causing the discrepancies. In addition, the preferred direction from the total sample (Chandra + XMM-Newton) is basically consistent with that from the Chandra and XMM-N observations.

In order to more intuitively understand these preferred directions of different datasets, we mapped the MCMC sampling results of preferred direction  $(l, b)$  in the galactic coordinate

system utilizing the `plt.contour()` function<sup>1</sup>, as shown in figure 10. The MCMC sampling results come from sampling based on the entire space of parameters  $l$  ( $-180^\circ \leq l \leq 180^\circ$ ). Color-coded values represent sample fraction per unit area. Larger values indicate tighter results. From figure 10, it can be seen that there are two preferred directions these two directions found in each galaxy cluster dataset. These two directions are almost symmetrical in the galactic coordinate system. It is easier to spot differences in preferred directions obtained from different datasets. We also marked the preferred directions obtained by truncating the prior range of the parameter  $l$  in figure 10. We can find that narrowing the prior bound on parameter  $l$  causes a slight shift (within  $1\sigma$  range) in the preferred direction. This indicates that changing the prior parameter space of  $l$  has little effect on the preferred direction. In addition, it should be noted here that the  $1\sigma$  error is not reflected in figure 10.

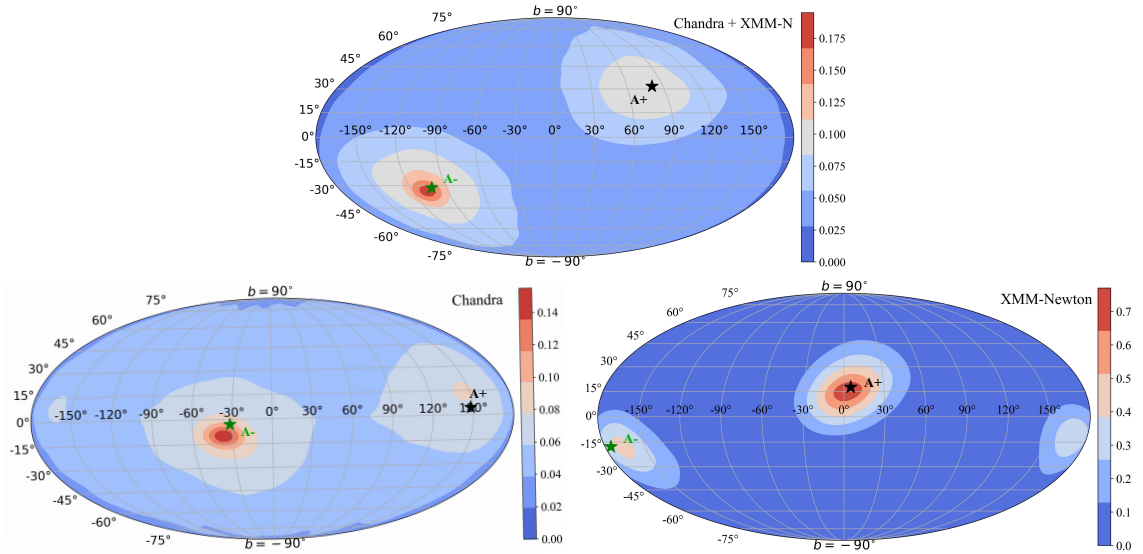


**Figure 10.** Preferred direction  $(l, b)$  in the galactic coordinate system. The contours show the MCMC sampling results come from sampling based on the entire space of parameters  $l$  ( $-180^\circ \leq l \leq 180^\circ$ ). The stars represent the preferred directions obtained by truncating the prior range of the parameter  $l$ . Green and black represent preferred directions of faster ( $A-$ ) and slower ( $A+$ ) expansion, respectively.

Through investigating the results of different redshift subsamples, we can find that there are actually large differences between the preferred directions and the level of cosmic anisotropy. For the preferred direction  $(l, b)$ , these two datasets differ by  $107.83^\circ$  in longitude  $l$  and  $41.14^\circ$  in latitude  $b$ . The results obtained from LR dataset are in line with those obtained from the total sample, and are consistent with the results obtained from the Chandra dataset within  $1\sigma$  level. While the results obtained from the HR dataset are consistent with that from the XMM-Newton dataset within  $1\sigma$  level. To more intuitively understand the differences between the preferred directions of different redshift datasets, we utilized the same processing method as figure 10 to map the MCMC sampling results of preferred direction  $(l, b)$ , as shown in figure 11. For the anisotropic level, the high-redshift observations (HR dataset) give a stronger signal of cosmic anisotropy. From the comparison of the results of the two datasets in figure 7, we can understand these findings more directly. These findings mean

<sup>1</sup>[https://matplotlib.org/stable/gallery/images\\_contours\\_and\\_fields/irregulardatagrid.html](https://matplotlib.org/stable/gallery/images_contours_and_fields/irregulardatagrid.html)

that cosmic anisotropy might evolve with redshift. It is possible that this might be caused by differences in the uniformity of the spatial distribution of the observations at different redshifts. The uniformity of the HR dataset across the sky is worse than that of the LR dataset. Therefore, there is reason to suspect that the uneven spatial distribution of HR dataset affects the preferred directions and level of cosmic anisotropy.

To clarify the effect of inhomogeneity on the anisotropic signal and examine whether dipole correction parameter  $A$  are consistent with statistical isotropy, we also performed statistical analyses for the different datasets. The statistical results are described in detail in Section 4.4 and listed in table 3. For the Mock scheme, we preserved the spatial distribution of the real data. According to the statistical results ( $\mu_{A_{mock}}$ ), we find that the anisotropy level provided by the non-uniform distribution of galaxy clusters is relatively weak, lower than ( $10^{-6} \sim 10^{-5}$ ), which is significantly lower than the real data ( $10^{-4} \sim 10^{-3}$ ). This indicates that the level of anisotropy reflected in the real data is largely contributed by the non-uniformity of the cosmic structure. To further examine the impact of non-uniform data distribution, we also considered the Iso scheme, which places the real data evenly on the celestial sphere. In theory, uniform simulation data can yield lower values of ( $\mu_{A_{mock}}$ ) that reflect a lower level of anisotropy. By comparing the statistical results of the two schemes (Mock and Iso), we find that uniformly simulated data did indeed achieve a lower level of anisotropy. However, this phenomenon is only observed in the Chandra, XMM-Newton, and LR datasets, while the statistical results ( $\mu_{A_{mock}}$ ) for Chandra + XMM-N (total) and HR datasets show a slight increase. This suggests that there are other factors in galaxy clusters that might cause anisotropy, and their contribution to anisotropy is comparable to the uniformity of the spatial distribution of the data. By marking the  $A$ -values obtained from the real data in the statistical results, we can obtain the statistical significance of the real data. Ultimately, the maximum statistical significance obtained by the two schemes are  $2.26\sigma$  (Mock) and  $2.86\sigma$  (Iso), respectively, both derived from the XMM-Newton dataset. The statistical significance of anisotropy obtained from galaxy clusters is significantly lower than that from SNe Ia [more than  $4\sigma$ ; 129, 137]. This may be due to a variety of factors, including data type, spatial distribution, and research methods. If we can use other studies to precisely restrict the preferred direction of anisotropy, could we improve the significance of anisotropy? To verify this idea, we first fixed the preferred direction as the best fit and then re-constrained the correction parameters  $A$  and  $B$  independently. To verify this idea, we first fixed the preferred directions as the best fits and then independently constrained the correction parameters  $A$  and  $B$ . We find that fixing the preferred direction significantly increased the anisotropy level (the value of  $A$ ) obtained from different datasets. Parameter  $B$  does not exhibit this consistent behavior. We label these results as  $A^*$  and  $B^*$ , and collect the constraints in table 2. We then combined the obtained  $A^*$  values with the statistical isotropy results and find that the statistical significance  $D_{fix}$  was significantly improved. The statistical significance of the two schemes increased from  $2.26\sigma$  (Mock) and  $2.86\sigma$  (Iso) to  $2.89\sigma$  (Mock) and  $3.64\sigma$  (Iso). All numerical results are presented in table 3.

At the end of the section, we also compared our findings with those of previous researches. First, we compared the preferred directions obtained from the galaxy clusters by a different method. The preferred directions from the Chandra, LR and Chandra + XMM-Newton datasets are consistent with the results from [68] within  $1\sigma$  level. Utilizing the sky scanning method, they found strong anisotropies toward Galactic coordinates ( $280^\circ$ ,  $-20^\circ$ ) and ( $303^\circ$ ,  $-27^\circ$ ) from 313 galaxy clusters and 842 galaxy clusters, respectively. After that, we compared our results with those from other observations, including CMB dipole [173, 174],

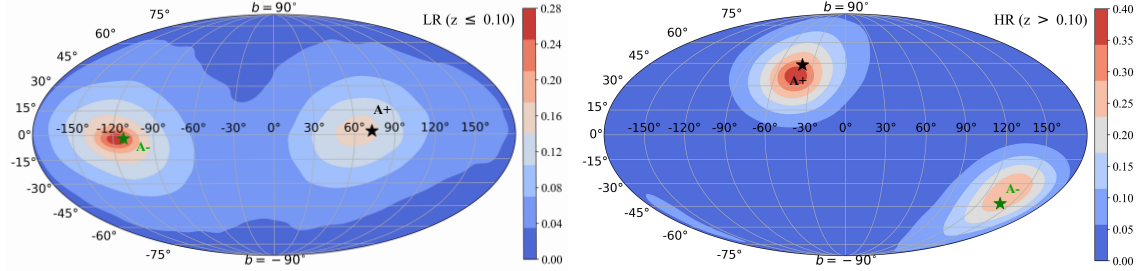


**Figure 11.** Preferred direction ( $l, b$ ) in the galactic coordinate system. The contours show the MCMC sampling results come from sampling based on the entire space of parameters  $l$  ( $-180^\circ \leq l \leq 180^\circ$ ). The stars represent the preferred directions obtained by truncating the prior range of the parameter  $l$ . Green and black represent preferred directions of faster ( $A-$ ) and slower ( $A+$ ) expansion, respectively.

bulk flow [175–177], dark flow [66], Pantheon [82], Pantheon+ [129, 137], GRB [111], SN + Quasar [121]. It is easy to find that the preferred directions corresponding to faster expansion from the Chandra, LR and total datasets are in line with the most of observations, except for the CMB dipole [173, 174] and SN + Quasar [121]. But the preferred direction corresponding to slower expansion from the HR ( $z > 0.10$ ) is consistent with that from the CMB dipole [173, 174] and SN + Quasar [121]. The preferred directions (faster) obtained from the XMM-Newton and HR datasets are quite different from previous studies. To facilitate understanding, we aggregated these results with the ones we obtained, marking them on the galactic coordinate system, as shown in figure 12.

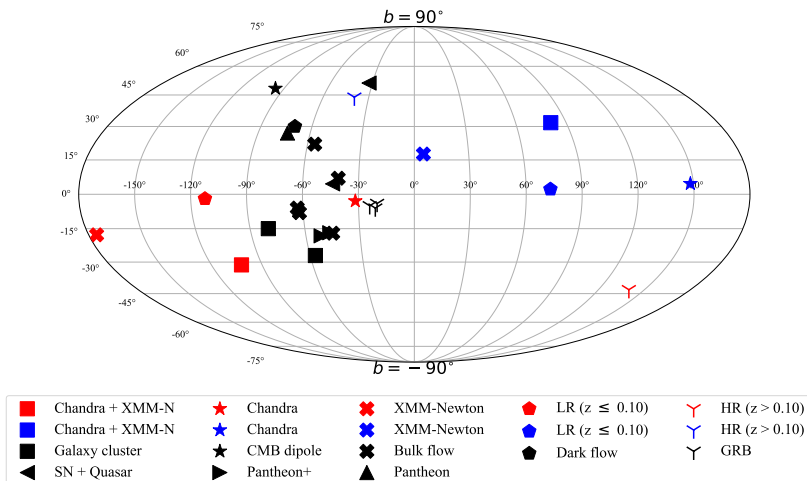


**Figure 12.** Distribution of preferred directions ( $l, b$ ) from the previous researches. The color represents the important result obtained in this work; red and blue represent preferred directions of faster and slower expansion, respectively. Black shows the result given by other independent observations including the galaxy cluster [94], CMB dipole [173, 174], bulk flow [175–177], dark flow [66], GRB [111], SN + Quasar [121], Pantheon+ [129, 137] and Pantheon [82].

**Table 2.** Best fitting results of the correction parameter ( $l$ ,  $b$ ,  $A$  and  $B$ ) from different datasets. The symbol \* represents  $A$  and  $B$  when the preferred direction ( $l$ ,  $b$ ) fixed as the best fitting results.

Sample	$l$	$b$	$A$	$B$	$A^*$	$B^*$
	[ $^{\circ}$ ]	[ $^{\circ}$ ]	$\times 10^{-4}$	$\times 10^{-4}$	$\times 10^{-4}$	$\times 10^{-4}$
Chandra	$328.31^{+66.52}_{-63.56}$	$-2.91^{+57.78}_{-52.27}$	$-1.9^{+6.8}_{-6.2}$	$-0.6 \pm 3.7$	$-5.9 \pm 7.5$	$-0.3 \pm 3.6$
	$148.32^{+60.16}_{-57.50}$	$4.62^{+51.70}_{-57.03}$	$2.2^{+6.1}_{-6.8}$	$-0.6 \pm 3.7$	$5.9 \pm 7.5$	$-0.3 \pm 3.7$
XMM-Newton	$184.42^{+29.01}_{-24.58}$	$-17.73^{+18.55}_{-21.53}$	$-32.0^{+15.0}_{-18.0}$	$-3.9 \pm 8.1$	$-41 \pm 14$	$-5.8 \pm 6.6$
	$5.0^{+28.81}_{-25.33}$	$17.61^{+21.56}_{-18.68}$	$32.0^{+18.0}_{-15.0}$	$-3.9 \pm 8.0$	$42 \pm 13$	$-5.7 \pm 6.6$
Chandra + XMM-N	$257.82^{+58.01}_{-52.88}$	$-31.30^{+35.92}_{-39.46}$	$-5.4 \pm 6.3$	$0.5 \pm 3.2$	$-8.8 \pm 5.7$	$0.5 \pm 3.2$
	$80.89^{+60.97}_{-52.46}$	$31.75^{+35.19}_{-40.16}$	$5.2^{+6.5}_{-5.8}$	$0.4 \pm 3.2$	$8.7 \pm 5.7$	$0.6 \pm 3.2$
LR ( $z \leq 0.10$ )	$247.66^{+58.30}_{-49.20}$	$-1.93^{+45.43}_{-43.45}$	$-6.5^{+9.7}_{-8.0}$	$-0.9 \pm 4.2$	$-14.1 \pm 8.3$	$-0.9 \pm 4.1$
	$73.01^{+62.39}_{-46.50}$	$2.21^{+42.77}_{-44.55}$	$6.6^{+8.3}_{-9.6}$	$-0.8 \pm 4.2$	$13.7 \pm 8.2$	$-0.7 \pm 4.1$
HR ( $z > 0.10$ )	$139.84^{+39.62}_{-35.47}$	$-43.07^{+21.52}_{-25.53}$	$-16.2^{+9.0}_{-8.1}$	$-2.6 \pm 4.2$	$-20.5 \pm 7.8$	$-3.3 \pm 4.2$
	$320.57^{+40.04}_{-35.15}$	$43.90^{+25.52}_{-21.64}$	$16.3 \pm 8.8$	$-2.5 \pm 4.3$	$20.4 \pm 7.7$	$-3.2 \pm 4.2$

**Table 3.** Statistical isotropic analysis results.  $\mu_{A_{mock}}$  represents the expected value and standard deviation of the statistical isotropic results.  $D_{free}$  and  $D_{fix}$  represent the statistical significance of the real data. The former is derived from  $A$  obtained from the real data, and the latter is derived from  $A^*$ .

Sample	Mock scheme			Iso scheme		
	$\mu_{A_{mock}}$ $\times 10^{-5}$	$D_{free}$ ( $\sigma$ )	$D_{fix}$ ( $\sigma$ )	$\mu_{A_{mock}}$ $\times 10^{-5}$	$D_{free}$ ( $\sigma$ )	$D_{fix}$ ( $\sigma$ )
Chandra	$-3.1 \pm 77.1$	0.20	0.75	$2.2 \pm 67.6$	0.30	0.90
XMM-Newton	$5.5 \pm 143.9$	2.26	2.89	$4.0 \pm 113.8$	2.86	3.64
Chandra + XMM-N	$-0.1 \pm 59.5$	0.93	1.48	$-2.0 \pm 59.6$	0.91	1.46
LR ( $z \leq 0.10$ )	$-2.0 \pm 86.8$	0.71	1.60	$-0.3 \pm 74.3$	0.87	1.90
HR ( $z > 0.10$ )	$-1.5 \pm 82.0$	1.97	2.48	$4.8 \pm 71.9$	2.31	2.93

## 6 Summary

In this paper, we utilize the DF method to the galaxy cluster for the first time to search for the preferred direction of the cosmic anisotropy. By leveraging  $L_X - T$  correlation, we were able to apply the DF method to galaxy cluster. From the Chandra + XMM-Newton dataset, we find two preferred directions ( $257.82^{\circ +58.01}_{-52.88}$ ,  $-31.30^{\circ +35.92}_{-39.46}$ ; faster) and ( $80.89^{\circ +60.97}_{-52.46}$ ,  $31.75^{\circ +35.19}_{-40.16}$ , slower) with corresponding anisotropy levels ( $A$ ) of  $-5.4 \pm 6.3 \times 10^{-4}$  and  $5.2^{+6.5}_{-5.8} \times 10^{-4}$ , respectively. Analysis of subsamples from different observation instruments (Chandra and XMM-Newton) revealed that the instrumentation influences the preferred direction and anisotropic level. The galaxy cluster subsamples from the XMM-Newton satellite exhibited more significant anisotropy. Meanwhile, we also divided the total sample into low redshift and high redshift subsamples (LR and HR) based on a redshift of 0.10, and discussed the impact of redshift on the anisotropy results. From the constraints, it is easy to find that the high redshift (HR) dataset gives a stronger signal of cosmic anisotropy than that from low redshift (LR). This hints that cosmic anisotropy might evolve with redshift.

In order to examine whether the anisotropic level from the galaxy clusters is consistent with statistical isotropy, we constructed two statistical isotropy analysis schemes: Mock scheme and Iso scheme. The statistical results indicate that the level of anisotropy contributed by the non-uniformity of the spatial distribution of the data is much lower than that of the actual data. This suggests that anisotropic signals are more likely to originate from the non-uniformity of the cosmic structure. By comparing the statistical results of the two schemes (Mock and Iso), we find that the uniformly simulated data (Iso) in the Chandra, XMM-Newton and LR datasets give a lower level of anisotropy, while the Chandra + XMM-N and HR datasets show the opposite. This suggests that there are other factors in galaxy clusters that might cause anisotropy, and their contribution to anisotropy is comparable to the uniformity of the spatial distribution of the data. The maximum statistical significance obtained by the two schemes are  $2.26\sigma$  (Mock) and  $2.86\sigma$  (Iso), respectively, both derived from the XMM-Newton dataset. Subsequently, we reanalyzed the galaxy cluster datasets by fixing the preferred direction ( $l, b$ ) as the best fits and find that if the preferred direction can be determined independently in other ways, more obvious anisotropic signals can be found in the galaxy clusters.

Overall, the DF method can be well integrated with galaxy clusters and applied to the detection of cosmic anisotropy. Our research provides a new scheme to construct a statistical analyses for the DF method, which is commonly used to test cosmological principle. Final results indicate the presence of anisotropic signals within galaxy clusters. In the future, we can further confirm and understand this signal using high-quality galaxy cluster data from the e-ROSITA [178–181].

## Acknowledgements

This work was supported by the National Natural Science Foundation of China (grant No. No. 12494575, 12273009, No. 12373026, No. 12003020) and Shaanxi Fundamental Science Research Project for Mathematics and Physics (grant No. 23JSY015).

## References

- [1] D.M. Scolnic, D.O. Jones, A. Rest, Y.C. Pan, R. Chornock, R.J. Foley et al., *The Complete Light-curve Sample of Spectroscopically Confirmed SNe Ia from Pan-STARRS1 and*

*Cosmological Constraints from the Combined Pantheon Sample*, *ApJ* **859** (2018) 101 [[1710.00845](#)].

[2] T.M.C. Abbott, A. Alarcon, S. Allam, P. Andersen, F. Andrade-Oliveira, J. Annis et al., *Cosmological Constraints from Multiple Probes in the Dark Energy Survey*, *Phys. Rev. Lett.* **122** (2019) 171301 [[1811.02375](#)].

[3] N. Khadka and B. Ratra, *Quasar X-ray and UV flux, baryon acoustic oscillation, and Hubble parameter measurement constraints on cosmological model parameters*, *MNRAS* **492** (2020) 4456 [[1909.01400](#)].

[4] D. Brout, D. Scolnic, B. Popovic, A.G. Riess, A. Carr, J. Zuntz et al., *The Pantheon+ Analysis: Cosmological Constraints*, *ApJ* **938** (2022) 110 [[2202.04077](#)].

[5] S. Cao and B. Ratra, *Using lower redshift, non-CMB, data to constrain the Hubble constant and other cosmological parameters*, *MNRAS* **513** (2022) 5686 [[2203.10825](#)].

[6] M.G. Dainotti, V. Nielson, G. Sarracino, E. Rinaldi, S. Nagataki, S. Capozziello et al., *Optical and X-ray GRB Fundamental Planes as cosmological distance indicators*, *MNRAS* **514** (2022) 1828 [[2203.15538](#)].

[7] X.D. Jia, J.P. Hu, J. Yang, B.B. Zhang and F.Y. Wang,  *$E_{iso}$ - $E_p$  correlation of gamma-ray bursts: calibration and cosmological applications*, *MNRAS* **516** (2022) 2575 [[2208.09272](#)].

[8] Y. Liu, F. Chen, N. Liang, Z. Yuan, H. Yu and P. Wu, *The Improved Amati Correlations from Gaussian Copula*, *ApJ* **931** (2022) 50 [[2203.03178](#)].

[9] N. Liang, Z. Li, X. Xie and P. Wu, *Calibrating Gamma-Ray Bursts by Using a Gaussian Process with Type Ia Supernovae*, *ApJ* **941** (2022) 84 [[2211.02473](#)].

[10] A. Porredon, M. Crocce, J. Elvin-Poole, R. Cawthon, G. Giannini, J. De Vicente et al., *Dark Energy Survey Year 3 results: Cosmological constraints from galaxy clustering and galaxy-galaxy lensing using the MAGLIM lens sample*, *Phys. Rev. D* **106** (2022) 103530 [[2105.13546](#)].

[11] F.Y. Wang, J.P. Hu, G.Q. Zhang and Z.G. Dai, *Standardized Long Gamma-Ray Bursts as a Cosmic Distance Indicator*, *ApJ* **924** (2022) 97 [[2106.14155](#)].

[12] J. de Cruz Pérez, C.-G. Park and B. Ratra, *Current data are consistent with flat spatial hypersurfaces in the  $\Lambda$  CDM cosmological model but favor more lensing than the model predicts*, *Phys. Rev. D* **107** (2023) 063522 [[2211.04268](#)].

[13] N. Khadka, M. Zajaček, R. Prince, S. Panda, B. Czerny, M.L. Martínez-Aldama et al., *Quasar UV/X-ray relation luminosity distances are shorter than reverberation-measured radius-luminosity relation luminosity distances*, *MNRAS* **522** (2023) 1247 [[2212.10483](#)].

[14] Z. Li, B. Zhang and N. Liang, *Testing dark energy models with gamma-ray bursts calibrated from the observational  $H(z)$  data through a Gaussian process*, *MNRAS* **521** (2023) 4406 [[2212.14291](#)].

[15] D. Rubin, G. Aldering, M. Betoule, A. Fruchter, X. Huang, A.G. Kim et al., *Union Through UNITY: Cosmology with 2,000 SNe Using a Unified Bayesian Framework*, *arXiv e-prints* (2023) arXiv:2311.12098 [[2311.12098](#)].

[16] A.G. Adame, J. Aguilar, S. Ahlen, S. Alam, D.M. Alexander, M. Alvarez et al., *DESI 2024 VI: cosmological constraints from the measurements of baryon acoustic oscillations*, *J. Cosmology Astropart. Phys.* **2025** (2025) 021 [[2404.03002](#)].

[17] L. Verde, T. Treu and A.G. Riess, *Tensions between the early and late Universe*, *Nature Astronomy* **3** (2019) 891 [[1907.10625](#)].

[18] A.G. Riess, *The expansion of the Universe is faster than expected*, *Nature Reviews Physics* **2** (2020) 10 [[2001.03624](#)].

[19] E. Di Valentino, O. Mena, S. Pan, L. Visinelli, W. Yang, A. Melchiorri et al., *In the realm of the Hubble tension-a review of solutions*, *Classical and Quantum Gravity* **38** (2021) 153001 [[2103.01183](#)].

[20] P. Shah, P. Lemos and O. Lahav, *A buyer’s guide to the Hubble constant*, *A&A Revie* **29** (2021) 9 [[2109.01161](#)].

[21] L. Perivolaropoulos and F. Skara, *Challenges for  $\Lambda$ CDM: An update*, *New Astron. Rev.* **95** (2022) 101659 [[2105.05208](#)].

[22] J.-P. Hu and F.-Y. Wang, *Hubble Tension: The Evidence of New Physics*, *Universe* **9** (2023) 94 [[2302.05709](#)].

[23] P. Kumar Aluri, P. Cea, P. Chingangbam, M.-C. Chu, R.G. Clowes, D. Hutsemékers et al., *Is the observable Universe consistent with the cosmological principle?*, *Classical and Quantum Gravity* **40** (2023) 094001.

[24] A.G. Riess and L. Breuval, *The Local Value of  $H_0$* , in *IAU Symposium*, R. de Grijs, P.A. Whitelock and M. Catelan, eds., vol. 376 of *IAU Symposium*, pp. 15–29, Jan., 2024, DOI [[2308.10954](#)].

[25] E. Di Valentino, L.A. Anchordoqui, Ö. Akarsu, Y. Ali-Haimoud, L. Amendola, N. Arendse et al., *Cosmology Intertwined III:  $f\sigma_8$  and  $S_8$* , *Astroparticle Physics* **131** (2021) 102604 [[2008.11285](#)].

[26] R.C. Nunes and S. Vagnozzi, *Arbitrating the  $S_8$  discrepancy with growth rate measurements from redshift-space distortions*, *MNRAS* **505** (2021) 5427 [[2106.01208](#)].

[27] S.A. Adil, Ö. Akarsu, M. Malekjani, E. Ó Colgáin, S. Pourojaghi, A.A. Sen et al.,  *$S_8$  increases with effective redshift in  $\Lambda$ CDM cosmology*, *MNRAS* **528** (2024) L20 [[2303.06928](#)].

[28] M. Hollis, *Hints of a physical origin for the  $S_8$  tension*, *Nature Astronomy* **8** (2024) 405.

[29] C. Stahl, B. Famaey, R. Ibata, O. Hahn, N. Martinet and T. Montandon, *Scale-dependent local primordial non-Gaussianity as a solution to the  $S_8$  tension*, *Phys. Rev. D* **110** (2024) 063501 [[2404.03244](#)].

[30] G.-B. Zhao, R.G. Crittenden, L. Pogosian and X. Zhang, *Examining the Evidence for Dynamical Dark Energy*, *Phys. Rev. Lett.* **109** (2012) 171301 [[1207.3804](#)].

[31] G.-B. Zhao, M. Raveri, L. Pogosian, Y. Wang, R.G. Crittenden, W.J. Handley et al., *Dynamical dark energy in light of the latest observations*, *Nature Astronomy* **1** (2017) 627 [[1701.08165](#)].

[32] E.Ó. Colgáin and M.M. Sheikh-Jabbari, *DESI and SNe: Dynamical Dark Energy,  $\Omega_m$  Tension or Systematics?*, *arXiv e-prints* (2024) arXiv:2412.12905 [[2412.12905](#)].

[33] M. Van Raamsdonk and C. Waddell, *Suggestions of decreasing dark energy from supernova and BAO data*, *J. Cosmology Astropart. Phys.* **2024** (2024) 047 [[2305.04946](#)].

[34] I. Tutzusaus, M. Kunz and L. Favre, *Solving the Hubble tension at intermediate redshifts with dynamical dark energy*, *arXiv e-prints* (2023) arXiv:2311.16862 [[2311.16862](#)].

[35] M. Lopez-Hernandez and J. De-Santiago, *Is there a dynamical tendency in  $H_0$  with late time measurements?*, *J. Cosmology Astropart. Phys.* **2025** (2025) 026 [[2411.00095](#)].

[36] A.N. Ormondroyd, W.J. Handley, M.P. Hobson and A.N. Lasenby, *Nonparametric reconstructions of dynamical dark energy via flexknots*, *arXiv e-prints* (2025) arXiv:2503.08658 [[2503.08658](#)].

[37] Y.-Y. Wang, Y.-J. Li and Y.-Z. Fan, *Evidence for the dynamical dark energy with evolving Hubble constant*, *arXiv e-prints* (2025) arXiv:2510.14390 [[2510.14390](#)].

[38] M. Scherer, M.A. Sabogal, R.C. Nunes and A. De Felice, *Challenging  $\Lambda$ CDM: 5 $\sigma$  Evidence for a Dynamical Dark Energy Late-Time Transition*, *arXiv e-prints* (2025) arXiv:2504.20664 [2504.20664].

[39] K.C. Wong, S.H. Suyu, G.C.F. Chen, C.E. Rusu, M. Millon, D. Sluse et al., *H0LiCOW - XIII. A 2.4 per cent measurement of  $H_0$  from lensed quasars: 5.3 $\sigma$  tension between early- and late-Universe probes*, *MNRAS* **498** (2020) 1420 [1907.04869].

[40] C. Krishnan, E.Ó. Colgáin, S. Ruchika, A. A., M.M. Sheikh-Jabbari and T. Yang, *Is there an early Universe solution to Hubble tension?*, *Phys. Rev. D* **102** (2020) 103525 [2002.06044].

[41] M.G. Dainotti, B. De Simone, T. Schiavone, G. Montani, E. Rinaldi and G. Lambiase, *On the Hubble Constant Tension in the SNe Ia Pantheon Sample*, *ApJ* **912** (2021) 150 [2103.02117].

[42] J.P. Hu and F.Y. Wang, *Revealing the late-time transition of  $H_0$ : relieve the Hubble crisis*, *MNRAS* **517** (2022) 576 [2203.13037].

[43] X.D. Jia, J.P. Hu and F.Y. Wang, *Evidence of a decreasing trend for the Hubble constant*, *A&A* **674** (2023) A45 [2212.00238].

[44] E. Ó Colgáin, M.M. Sheikh-Jabbari, R. Solomon, M.G. Dainotti and D. Stojkovic, *Putting flat  $\mathit{jmml:math altimg="si84.svg" display="inline" id="d1e4172" \mathit{jmml:mi}\mathit{\Lambda}\mathit{ji}/mml:mi}\mathit{\Lambda}\mathit{ji}/mml:math\mathit{\Lambda}\mathit{CDM}$  in the (Redshift) bin*, *Physics of the Dark Universe* **44** (2024) 101464 [2206.11447].

[45] X.D. Jia, J.P. Hu, S.X. Yi and F.Y. Wang, *Uncorrelated Estimations of  $H_0$  Redshift Evolution from DESI Baryon Acoustic Oscillation Observations*, *ApJ lett.* **979** (2025) L34 [2406.02019].

[46] S. Mazurenko, I. Banik and P. Kroupa, *The redshift dependence of the inferred  $H_0$  in a local void solution to the Hubble tension*, *MNRAS* **536** (2025) 3232 [2412.12245].

[47] S. Basilakos and S. Nesseris, *Conjoined constraints on modified gravity from the expansion history and cosmic growth*, *Phys. Rev. D* **96** (2017) 063517 [1705.08797].

[48] T.M.C. Abbott, F.B. Abdalla, A. Alarcon, J. Aleksić, S. Allam, S. Allen et al., *Dark Energy Survey year 1 results: Cosmological constraints from galaxy clustering and weak lensing*, *Phys. Rev. D* **98** (2018) 043526 [1708.01530].

[49] S. Joudaki, C. Blake, A. Johnson, A. Amon, M. Asgari, A. Choi et al., *KiDS-450 + 2dFLenS: Cosmological parameter constraints from weak gravitational lensing tomography and overlapping redshift-space galaxy clustering*, *MNRAS* **474** (2018) 4894 [1707.06627].

[50] L. Verde, P. Protopapas and R. Jimenez, *Planck and the local Universe: Quantifying the tension*, *Physics of the Dark Universe* **2** (2013) 166 [1306.6766].

[51] R. Jimenez, A. Cimatti, L. Verde, M. Moresco and B. Wandelt, *The local and distant Universe: stellar ages and  $H_0$* , *J. Cosmology Astropart. Phys.* **2019** (2019) 043 [1902.07081].

[52] J. Evslin, *Isolating the Lyman alpha forest BAO anomaly*, *J. Cosmology Astropart. Phys.* **2017** (2017) 024 [1604.02809].

[53] G.E. Addison, D.J. Watts, C.L. Bennett, M. Halpern, G. Hinshaw and J.L. Weiland, *Elucidating  $\Lambda$ CDM: Impact of Baryon Acoustic Oscillation Measurements on the Hubble Constant Discrepancy*, *ApJ* **853** (2018) 119 [1707.06547].

[54] A. Cuceu, J. Farr, P. Lemos and A. Font-Ribera, *Baryon Acoustic Oscillations and the Hubble constant: past, present and future*, *J. Cosmology Astropart. Phys.* **2019** (2019) 044 [1906.11628].

[55] J.S. Bullock and M. Boylan-Kolchin, *Small-Scale Challenges to the  $\Lambda$ CDM Paradigm*, *ARA&A* **55** (2017) 343 [1707.04256].

[56] P. Salucci, *The distribution of dark matter in galaxies*, *A&A Revie* **27** (2019) 2 [1811.08843].

[57] C.L. Bennett, M. Halpern, G. Hinshaw, N. Jarosik, A. Kogut, M. Limon et al., *First-Year Wilkinson Microwave Anisotropy Probe (WMAP) Observations: Preliminary Maps and Basic Results*, *ApJS* **148** (2003) 1 [[astro-ph/0302207](#)].

[58] D. Hutsemékers, R. Cabanac, H. Lamy and D. Sluse, *Mapping extreme-scale alignments of quasar polarization vectors*, *A&A* **441** (2005) 915 [[astro-ph/0507274](#)].

[59] C. Bonvin, R. Durrer and M. Kunz, *Dipole of the Luminosity Distance: A Direct Measure of  $H(z)$* , *Phys. Rev. Lett.* **96** (2006) 191302 [[astro-ph/0603240](#)].

[60] T. Koivisto and D.F. Mota, *Anisotropic dark energy: dynamics of the background and perturbations*, *J. Cosmology Astropart. Phys.* **2008** (2008) 018 [[0801.3676](#)].

[61] J. Colin, R. Mohayaee, S. Sarkar and A. Shafieloo, *Probing the anisotropic local Universe and beyond with SNe Ia data*, *MNRAS* **414** (2011) 264 [[1011.6292](#)].

[62] J.K. Webb, J.A. King, M.T. Murphy, V.V. Flambaum, R.F. Carswell and M.B. Bainbridge, *Indications of a Spatial Variation of the Fine Structure Constant*, *Phys. Rev. Lett.* **107** (2011) 191101 [[1008.3907](#)].

[63] M. Rubart, D. Bacon and D.J. Schwarz, *Impact of local structure on the cosmic radio dipole*, *A&A* **565** (2014) A111 [[1402.0376](#)].

[64] Ö. Akarsu, J.D. Barrow and N.M. Uzun, *Screening anisotropy via energy-momentum squared gravity: A CDM model with hidden anisotropy*, *Phys. Rev. D* **102** (2020) 124059 [[2009.06517](#)].

[65] C. Krishnan, R. Mondol and M.M. Sheikh-Jabbari, *Dipole cosmology: the Copernican paradigm beyond FLRW*, *J. Cosmology Astropart. Phys.* **2023** (2023) 020 [[2209.14918](#)].

[66] E. Abdalla, G.F. Abellán, A. Aboubrahim, A. Agnello, Ö. Akarsu, Y. Akrami et al., *Cosmology intertwined: A review of the particle physics, astrophysics, and cosmology associated with the cosmological tensions and anomalies*, *Journal of High Energy Astrophysics* **34** (2022) 49 [[2203.06142](#)].

[67] E. Di Valentino, J. Levi Said, A. Riess, A. Pollo, V. Poulin, A. Gómez-Valent et al., *The CosmoVerse White Paper: Addressing observational tensions in cosmology with systematics and fundamental physics*, *arXiv e-prints* (2025) arXiv:2504.01669 [[2504.01669](#)].

[68] K. Migkas, G. Schellenberger, T.H. Reiprich, F. Pacaud, M.E. Ramos-Ceja and L. Lovisari, *Probing cosmic isotropy with a new X-ray galaxy cluster sample through the  $L_X$ - $T$  scaling relation*, *A&A* **636** (2020) A15 [[2004.03305](#)].

[69] M. Tegmark, A. de Oliveira-Costa and A.J. Hamilton, *High resolution foreground cleaned CMB map from WMAP*, *Phys. Rev. D* **68** (2003) 123523 [[astro-ph/0302496](#)].

[70] P. Bielewicz, K.M. Górska and A.J. Banday, *Low-order multipole maps of cosmic microwave background anisotropy derived from WMAP*, *MNRAS* **355** (2004) 1283 [[astro-ph/0405007](#)].

[71] C.L. Bennett, R.S. Hill, G. Hinshaw, D. Larson, K.M. Smith, J. Dunkley et al., *Seven-year Wilkinson Microwave Anisotropy Probe (WMAP) Observations: Are There Cosmic Microwave Background Anomalies?*, *ApJS* **192** (2011) 17 [[1001.4758](#)].

[72] A. Gruppuso, F. Finelli, P. Natoli, F. Paci, P. Cabella, A. de Rosa et al., *New constraints on parity symmetry from a re-analysis of the WMAP-7 low-resolution power spectra*, *MNRAS* **411** (2011) 1445 [[1006.1979](#)].

[73] S. Ghosh and P. Jain, *A pixel space method for testing dipole modulation in the CMB polarization*, *MNRAS* **492** (2020) 3994 [[1807.02359](#)].

[74] Planck Collaboration, Y. Akrami, M. Ashdown, J. Aumont, C. Baccigalupi, M. Ballardini et al., *Planck 2018 results. VII. Isotropy and statistics of the CMB*, *A&A* **641** (2020) A7 [[1906.02552](#)].

[75] J.A. King, J.K. Webb, M.T. Murphy, V.V. Flambaum, R.F. Carswell, M.B. Bainbridge et al., *Spatial variation in the fine-structure constant - new results from VLT/UVES*, *MNRAS* **422** (2012) 3370 [[1202.4758](#)].

[76] X. Li and H.-N. Lin, *Spatial and temporal variations of the fine-structure constant in the Finslerian universe*, *Chinese Physics C* **41** (2017) 065102.

[77] D. Milaković, C.C. Lee, P. Molaro and J.K. Webb, *Methods for quasar absorption system measurements of the fine structure constant in the 2020s and beyond*, in *Memorie della Societa Astronomica Italiana*, vol. 94, p. 270, Sept., 2023, DOI [[2212.02458](#)].

[78] S.M. Koksbang, *Searching for Signals of Inhomogeneity Using Multiple Probes of the Cosmic Expansion Rate  $H(z)$* , *Phys. Rev. Lett.* **126** (2021) 231101 [[2105.11880](#)].

[79] A. Mariano and L. Perivolaropoulos, *Is there correlation between fine structure and dark energy cosmic dipoles?*, *Phys. Rev. D* **86** (2012) 083517 [[1206.4055](#)].

[80] J. Bayron Orjuela-Quintana, M. Álvarez, C.A. Valenzuela-Toledo and Y. Rodríguez, *Anisotropic Einstein Yang-Mills Higgs dark energy*, *J. Cosmology Astropart. Phys.* **2020** (2020) 019 [[2006.14016](#)].

[81] J. Motoa-Manzano, J.B. Orjuela-Quintana, T.S. Pereira and C.A. Valenzuela-Toledo, *Anisotropic solid dark energy*, *Physics of the Dark Universe* **32** (2021) 100806 [[2012.09946](#)].

[82] L. Kazantzidis and L. Perivolaropoulos, *Hints of a local matter underdensity or modified gravity in the low  $z$  Pantheon data*, *Phys. Rev. D* **102** (2020) 023520 [[2004.02155](#)].

[83] O. Luongo, M. Muccino, E.Ó. Colgáin, M.M. Sheikh-Jabbari and L. Yin, *Larger  $H_0$  values in the CMB dipole direction*, *Phys. Rev. D* **105** (2022) 103510 [[2108.13228](#)].

[84] R. Mc Conville and E. Ó Colgáin, *Anisotropic distance ladder in Pantheon+supernovae*, *Phys. Rev. D* **108** (2023) 123533 [[2304.02718](#)].

[85] J. Colin, R. Mohayaee, M. Rameez and S. Sarkar, *High-redshift radio galaxies and divergence from the CMB dipole*, *MNRAS* **471** (2017) 1045 [[1703.09376](#)].

[86] A.K. Singal, *Large disparity in cosmic reference frames determined from the sky distributions of radio sources and the microwave background radiation*, *Phys. Rev. D* **100** (2019) 063501 [[1904.11362](#)].

[87] A.K. Singal, *Discordance of dipole asymmetries seen in recent large radio surveys with the cosmological principle*, *MNRAS* **524** (2023) 3636 [[2303.05141](#)].

[88] C.A.P. Bengaly, R. Maartens and M.G. Santos, *Probing the Cosmological Principle in the counts of radio galaxies at different frequencies*, *J. Cosmology Astropart. Phys.* **2018** (2018) 031 [[1710.08804](#)].

[89] M. Rameez, R. Mohayaee, S. Sarkar and J. Colin, *The dipole anisotropy of AllWISE galaxies*, *MNRAS* **477** (2018) 1772 [[1712.03444](#)].

[90] O.T. Oayda, V. Mittal, G.F. Lewis and T. Murphy, *A Bayesian approach to the cosmic dipole in radio galaxy surveys: joint analysis of NVSS & RACS*, *MNRAS* **531** (2024) 4545 [[2406.01871](#)].

[91] O.T. Oayda, V. Mittal and G.F. Lewis, *Cosmic multipoles in galaxy surveys - I. How inferences depend on source counts and masks*, *MNRAS* **537** (2025) 1 [[2412.12600](#)].

[92] D. Patel and H. Desmond, *No evidence for anisotropy in galaxy spin directions*, *MNRAS* **534** (2024) 1553 [[2404.06617](#)].

[93] K. Migkas and T.H. Reiprich, *Anisotropy of the galaxy cluster X-ray luminosity-temperature relation*, *A&A* **611** (2018) A50 [[1711.02539](#)].

[94] K. Migkas, F. Pacaud, G. Schellenberger, J. Erler, N.T. Nguyen-Dang, T.H. Reiprich et al., *Cosmological implications of the anisotropy of ten galaxy cluster scaling relations*, *A&A* **649** (2021) A151 [[2103.13904](#)].

[95] A. Pandya, K. Migkas, T.H. Reiprich, A. Stanford, F. Pacaud, G. Schellenberger et al., *Examining the local Universe isotropy with galaxy cluster velocity dispersion scaling relations*, *A&A* **691** (2024) A355 [[2408.00726](#)].

[96] K. Migkas, *Galaxy clusters as probes of cosmic isotropy*, *Philosophical Transactions of the Royal Society of London Series A* **383** (2025) 20240030 [[2406.01752](#)].

[97] Y. He, K. Migkas, J. Schaye, J. Braspenning and M. Schaller, *Characterising galaxy cluster scaling relations as cosmic isotropy tracers using the FLAMINGO simulations*, *arXiv e-prints* (2025) arXiv:2504.01745 [[2504.01745](#)].

[98] I.M.E. Santos-Santos, J.F. Navarro and A. McConnachie, *Anisotropies in the spatial distribution and kinematics of dwarf galaxies in the Local Group and beyond*, *MNRAS* **532** (2024) 2490 [[2310.02464](#)].

[99] V. Pelgrims and D. Hutsemékers, *Evidence for the alignment of quasar radio polarizations with large quasar group axes*, *A&A* **590** (2016) A53 [[1604.03937](#)].

[100] P. Tiwari and P. Jain, *Evidence of isotropy on large distance scales from polarizations of radio sources*, *A&A* **622** (2019) A113 [[1809.01270](#)].

[101] N.J. Secrest, S. von Hausegger, M. Rameez, R. Mohayaee, S. Sarkar and J. Colin, *A Test of the Cosmological Principle with Quasars*, *ApJ lett.* **908** (2021) L51 [[2009.14826](#)].

[102] D. Zhao and J.-Q. Xia, *A tomographic test of cosmic anisotropy with the recently-released quasar sample*, *European Physical Journal C* **81** (2021) 948.

[103] D. Zhao and J.-Q. Xia, *Constraining the anisotropy of the Universe with the X-ray and UV fluxes of quasars*, *European Physical Journal C* **81** (2021) 694 [[2105.03965](#)].

[104] L. Dam, G.F. Lewis and B.J. Brewer, *Testing the cosmological principle with CatWISE quasars: a bayesian analysis of the number-count dipole*, *MNRAS* **525** (2023) 231 [[2212.07733](#)].

[105] C. Guandalin, J. Piat, C. Clarkson and R. Maartens, *Theoretical Systematics in Testing the Cosmological Principle with the Kinematic Quasar Dipole*, *ApJ* **953** (2023) 144 [[2212.04925](#)].

[106] V. Mittal, O.T. Oayda and G.F. Lewis, *The cosmic dipole in the Quaia sample of quasars: a Bayesian analysis*, *MNRAS* **527** (2024) 8497 [[2311.14938](#)].

[107] O.T. Oayda, V. Mittal and G.F. Lewis, *Cosmic multipoles in galaxy surveys Part I: How inferences depend on source counts and masks*, *MNRAS* (2024) [[2412.12600](#)].

[108] M. Panwar and P. Jain, *Probing the cosmological principle using the slope of log N-log S relationship for quasars*, *J. Cosmology Astropart. Phys.* **2024** (2024) 019 [[2312.07596](#)].

[109] S.M. Koksbang, *Testing inhomogeneous cosmography in our cosmic neighborhood using CosmicFlows-4*, *arXiv e-prints* (2024) arXiv:2412.12637 [[2412.12637](#)].

[110] J.S. Wang and F.Y. Wang, *Probing the anisotropic expansion from supernovae and GRBs in a model-independent way*, *MNRAS* **443** (2014) 1680 [[1406.6448](#)].

[111] D. Zhao and J.-Q. Xia, *Testing cosmic anisotropy with the  $E_p$ - $E_{iso}$  ('Amati') correlation of GRBs*, *MNRAS* **511** (2022) 5661.

[112] J. Santiago, K. Asvesta, M.G. Dainotti and P. Chen, *Measuring cosmic dipole with the GRB luminosity-time relation*, *arXiv e-prints* (2025) arXiv:2510.20705 [[2510.20705](#)].

[113] R.-G. Cai, Y.-Z. Ma, B. Tang and Z.-L. Tuo, *Constraining the anisotropic expansion of the Universe*, *Phys. Rev. D* **87** (2013) 123522 [[1303.0961](#)].

[114] X. Yang, F.Y. Wang and Z. Chu, *Searching for a preferred direction with Union2.1 data*, *MNRAS* **437** (2014) 1840 [[1310.5211](#)].

[115] B. Javanmardi, C. Porciani, P. Kroupa and J. Pflamm-Altenburg, *Probing the Isotropy of Cosmic Acceleration Traced By Type Ia Supernovae*, *ApJ* **810** (2015) 47 [[1507.07560](#)].

[116] K. Migkas and M. Plionis, *Testing the isotropy of the Hubble expansion*, *Rev. Mex. Astron. Astrofis.* **52** (2016) 133 [[1602.02310](#)].

[117] H.-K. Deng and H. Wei, *Null signal for the cosmic anisotropy in the Pantheon supernovae data*, *European Physical Journal C* **78** (2018) 755 [[1806.02773](#)].

[118] Z.Q. Sun and F.Y. Wang, *Testing the anisotropy of cosmic acceleration from Pantheon supernovae sample*, *MNRAS* **478** (2018) 5153 [[1805.09195](#)].

[119] Y.-Y. Wang and F.Y. Wang, *Testing the isotropy of the Universe with Type Ia supernovae in a model-independent way*, *MNRAS* **474** (2018) 3516 [[1711.05974](#)].

[120] J. Colin, R. Mohayaee, M. Rameez and S. Sarkar, *Evidence for anisotropy of cosmic acceleration*, *A&A* **631** (2019) L13 [[1808.04597](#)].

[121] J.P. Hu, Y.Y. Wang and F.Y. Wang, *Testing cosmic anisotropy with Pantheon sample and quasars at high redshifts*, *A&A* **643** (2020) A93 [[2008.12439](#)].

[122] Ö. Akarsu, E. Di Valentino, S. Kumar, M. Özyigit and S. Sharma, *Testing spatial curvature and anisotropic expansion on top of the  $\Lambda$ CDM model*, *Physics of the Dark Universe* **39** (2023) 101162 [[2112.07807](#)].

[123] B. Kalbouneh, C. Marinoni and J. Bel, *Multipole expansion of the local expansion rate*, *Phys. Rev. D* **107** (2023) 023507 [[2210.11333](#)].

[124] P. da Silveira Ferreira and V. Marra, *Tomographic redshift dipole: testing the cosmological principle*, *J. Cosmology Astropart. Phys.* **2024** (2024) 077 [[2403.14580](#)].

[125] J.B. Orjuela-Quintana, J.L. Palacios-Córdoba and C.A. Valenzuela-Toledo, *Late-time anisotropy sourced by a 2-form field non-minimally coupled to cold dark matter*, *Physics of the Dark Universe* **46** (2024) 101575 [[2202.07546](#)].

[126] V. Yadav, *Measuring Hubble constant in an anisotropic extension of  $\Lambda$ CDM model*, *Physics of the Dark Universe* **42** (2023) 101365 [[2306.16135](#)].

[127] V. Yadav, S.K. Yadav and Rajpal, *Effects of anisotropy in an anisotropic extension of  $\mathcal{M}\mathcal{M}\mathcal{L}$ :  $\mathcal{M}\mathcal{M}\mathcal{L}$  model*, *Physics of the Dark Universe* **46** (2024) 101626 [[2402.16885](#)].

[128] J.P. Hu, X.D. Jia, J. Hu and F.Y. Wang, *Hints of New Physics for the Hubble Tension: Violation of Cosmological Principle*, *ApJ lett.* **975** (2024) L36 [[2410.06450](#)].

[129] J.P. Hu, Y.Y. Wang, J. Hu and F.Y. Wang, *Testing the cosmological principle with the Pantheon+ sample and the region-fitting method*, *A&A* **681** (2024) A88 [[2310.11727](#)].

[130] S. Mazurenko, I. Banik and P. Kroupa, *The redshift dependence of the inferred  $H_0$  in a local void solution to the Hubble tension*, *MNRAS* (2024) [[2412.12245](#)].

[131] C. Krishnan, R. Mohayaee, E.Ó. Colgáin, M.M. Sheikh-Jabbari and L. Yin, *Hints of FLRW breakdown from supernovae*, *Phys. Rev. D* **105** (2022) 063514 [[2106.02532](#)].

[132] W. Rahman, R. Trotta, S.S. Boruah, M.J. Hudson and D.A. van Dyk, *New constraints on anisotropic expansion from supernovae Type Ia*, *MNRAS* **514** (2022) 139 [[2108.12497](#)].

[133] N. Horstmann, Y. Pietschke and D.J. Schwarz, *Inference of the cosmic rest-frame from supernovae Ia*, *A&A* **668** (2022) A34 [[2111.03055](#)].

[134] Z. Zhai and W.J. Percival, *Sample variance for supernovae distance measurements and the Hubble tension*, *Phys. Rev. D* **106** (2022) 103527 [[2207.02373](#)].

[135] L. Tang, H.-N. Lin, L. Liu and X. Li, *Consistency of Pantheon+ supernovae with a large-scale isotropic universe*, *Chinese Physics C* **47** (2023) 125101 [[2309.11320](#)].

[136] C.A.P. Bengaly, J.S. Alcaniz and C. Pigozzo, *Testing the isotropy of cosmic acceleration with the Pantheon + and SH0ES datasets: A cosmographic analysis*, *Phys. Rev. D* **109** (2024) 123533 [[2402.17741](#)].

[137] J.P. Hu, J. Hu, X.D. Jia, B.Q. Gao and F.Y. Wang, *Testing cosmic anisotropy with Padé approximations and the latest Pantheon+ sample*, *A&A* **689** (2024) A215 [[2406.14827](#)].

[138] Z.-F. Yang, D.-W. Yao, M. Le Delliou and K. Wang, *Model-independent test of the cosmic anisotropy with inverse distance ladder*, *European Physical Journal C* **85** (2025) 339 [[2407.19278](#)].

[139] P. Boubel, M. Colless, K. Said and L. Staveley-Smith, *Testing anisotropic Hubble expansion*, *J. Cosmology Astropart. Phys.* **2025** (2025) 066 [[2412.14607](#)].

[140] R. Mokeddem, M. Lopes, F. Avila, A. Bernui and W.S. Hipólito-Ricaldi, *Probing cosmic isotropy: Hubble constant and matter density large-angle variations with the Pantheon+SH0ES data*, *arXiv e-prints* (2025) arXiv:2504.00903 [[2504.00903](#)].

[141] A. Sah, M. Rameez, S. Sarkar and C.G. Tsagas, *Anisotropy in Pantheon+ supernovae*, *European Physical Journal C* **85** (2025) 596 [[2411.10838](#)].

[142] D.J. Schwarz and B. Weinhorst, *(An)isotropy of the Hubble diagram: comparing hemispheres*, *A&A* **474** (2007) 717 [[0706.0165](#)].

[143] L. Perivolaropoulos, *Isotropy properties of the absolute luminosity magnitudes of SnIa in the Pantheon + and SH0ES samples*, *Phys. Rev. D* **108** (2023) 063509.

[144] Z. Chang, H.-N. Lin, Y. Sang and S. Wang, *A tomographic test of cosmological principle using the JLA compilation of type Ia supernovae*, *MNRAS* **478** (2018) 3633 [[1711.11321](#)].

[145] F. Sorrenti, R. Durrer and M. Kunz, *The dipole of the Pantheon+SH0ES data*, *J. Cosmology Astropart. Phys.* **2023** (2023) 054 [[2212.10328](#)].

[146] Y. Shen, G.T. Richards, M.A. Strauss, P.B. Hall, D.P. Schneider, S. Snedden et al., *A Catalog of Quasar Properties from Sloan Digital Sky Survey Data Release 7*, *ApJS* **194** (2011) 45 [[1006.5178](#)].

[147] U. Andrade, C.A.P. Bengaly, B. Santos and J.S. Alcaniz, *A Model-independent Test of Cosmic Isotropy with Low-z Pantheon Supernovae*, *ApJ* **865** (2018) 119 [[1806.06990](#)].

[148] D. Zhao, Y. Zhou and Z. Chang, *Anisotropy of the Universe via the Pantheon supernovae sample revisited*, *MNRAS* **486** (2019) 5679 [[1903.12401](#)].

[149] E. Lusso and G. Risaliti, *The Tight Relation between X-Ray and Ultraviolet Luminosity of Quasars*, *ApJ* **819** (2016) 154 [[1602.01090](#)].

[150] G. Risaliti and E. Lusso, *Cosmological Constraints from the Hubble Diagram of Quasars at High Redshifts*, *Nature Astronomy* **3** (2019) 272 [[1811.02590](#)].

[151] E. Lusso, G. Risaliti, E. Nardini, G. Bargiacchi, M. Benetti, S. Bisogni et al., *Quasars as standard candles. III. Validation of a new sample for cosmological studies*, *A&A* **642** (2020) A150 [[2008.08586](#)].

[152] R. Piffaretti, M. Arnaud, G.W. Pratt, E. Pointecouteau and J.B. Melin, *The MCXC: a meta-catalogue of x-ray detected clusters of galaxies*, *A&A* **534** (2011) A109 [[1007.1916](#)].

[153] H. Ebeling, A.C. Edge, S.W. Allen, C.S. Crawford, A.C. Fabian and J.P. Huchra, *The ROSAT Brightest Cluster Sample - IV. The extended sample*, *MNRAS* **318** (2000) 333 [[astro-ph/0003191](#)].

[154] H. Böhringer, W. Voges, J.P. Huchra, B. McLean, R. Giacconi, P. Rosati et al., *The Northern ROSAT All-Sky (NORAS) Galaxy Cluster Survey. I. X-Ray Properties of Clusters Detected as Extended X-Ray Sources*, *ApJS* **129** (2000) 435 [[astro-ph/0003219](#)].

[155] H. Böhringer, P. Schuecker, L. Guzzo, C.A. Collins, W. Voges, R.G. Cruddace et al., *The ROSAT-ESO Flux Limited X-ray (REFLEX) Galaxy cluster survey. V. The cluster catalogue*, *A&A* **425** (2004) 367 [[astro-ph/0405546](#)].

[156] W. Voges, B. Aschenbach, T. Boller, H. Bräuninger, U. Briel, W. Burkert et al., *The ROSAT all-sky survey bright source catalogue*, *A&A* **349** (1999) 389 [[astro-ph/9909315](#)].

[157] M.C. Weisskopf, H.D. Tananbaum, L.P. Van Speybroeck and S.L. O'Dell, *Chandra X-ray Observatory (CXO): overview*, in *X-Ray Optics, Instruments, and Missions III*, J.E. Truemper and B. Aschenbach, eds., vol. 4012 of *Society of Photo-Optical Instrumentation Engineers (SPIE) Conference Series*, pp. 2–16, July, 2000, DOI [[astro-ph/0004127](#)].

[158] F. Jansen, D. Lumb, B. Altieri, J. Clavel, M. Ehle, C. Erd et al., *XMM-Newton observatory. I. The spacecraft and operations*, *A&A* **365** (2001) L1.

[159] N. Kaiser, *Evolution and clustering of rich clusters.*, *MNRAS* **222** (1986) 323.

[160] A. Vikhlinin, L. van Speybroeck, M. Markevitch, W.R. Forman and L. Grego, *Evolution of the Cluster X-Ray Scaling Relations since  $z \gtrsim 0.4$* , *ApJ lett.* **578** (2002) L107 [[astro-ph/0207445](#)].

[161] F. Pacaud, M. Pierre, C. Adami, B. Altieri, S. Andreon, L. Chiappetti et al., *The XMM-LSS survey: the Class 1 cluster sample over the initial 5 deg<sup>2</sup> and its cosmological modelling*, *MNRAS* **382** (2007) 1289 [[0709.1950](#)].

[162] G.W. Pratt, J.H. Croston, M. Arnaud and H. Böhringer, *Galaxy cluster X-ray luminosity scaling relations from a representative local sample (REXCESS)*, *A&A* **498** (2009) 361 [[0809.3784](#)].

[163] R. Mittal, A. Hicks, T.H. Reiprich and V. Jaritz, *The  $L_X$  -  $T_{vir}$  relation in galaxy clusters: effects of radiative cooling and AGN heating*, *A&A* **532** (2011) A133 [[1106.5185](#)].

[164] A. Reichert, H. Böhringer, R. Fassbender and M. Mühlegger, *Observational constraints on the redshift evolution of X-ray scaling relations of galaxy clusters out to  $z \sim 1.5$* , *A&A* **535** (2011) A4 [[1109.3708](#)].

[165] M. Hilton, A.K. Romer, S.T. Kay, N. Mehrtens, E.J. Lloyd-Davies, P.A. Thomas et al., *The XMM Cluster Survey: evidence for energy injection at high redshift from evolution of the X-ray luminosity-temperature relation*, *MNRAS* **424** (2012) 2086 [[1205.5570](#)].

[166] B.J. Maughan, P.A. Giles, S.W. Randall, C. Jones and W.R. Forman, *Self-similar scaling and evolution in the galaxy cluster X-ray luminosity-temperature relation*, *MNRAS* **421** (2012) 1583 [[1108.1200](#)].

[167] V. Bharadwaj, T.H. Reiprich, L. Lovisari and H.J. Eckmiller, *Extending the  $L_X$  -  $T$  relation from clusters to groups. Impact of cool core nature, AGN feedback, and selection effects*, *A&A* **573** (2015) A75 [[1410.5428](#)].

[168] L. Lovisari, T.H. Reiprich and G. Schellenberger, *Scaling properties of a complete X-ray selected galaxy group sample*, *A&A* **573** (2015) A118 [[1409.3845](#)].

[169] P.A. Giles, B.J. Maughan, F. Pacaud, M. Lieu, N. Clerc, M. Pierre et al., *The XXL Survey. III. Luminosity-temperature relation of the bright cluster sample*, *A&A* **592** (2016) A3 [[1512.03833](#)].

[170] S. Zou, B.J. Maughan, P.A. Giles, A. Vikhlinin, F. Pacaud, R. Burenin et al., *The X-ray luminosity-temperature relation of a complete sample of low-mass galaxy clusters*, *MNRAS* **463** (2016) 820 [[1610.07674](#)].

- [171] Z. Chang, H.-N. Lin, Z.-C. Zhao and Y. Zhou, *Searching for a possible dipole anisotropy in acceleration scale with 147 rotationally supported galaxies*, *Chinese Physics C* **42** (2018) 115103 [[1803.08344](#)].
- [172] H.-K. Deng and H. Wei, *Testing the cosmic anisotropy with supernovae data: Hemisphere comparison and dipole fitting*, *Phys. Rev. D* **97** (2018) 123515 [[1804.03087](#)].
- [173] Planck Collaboration, R. Adam, P.A.R. Ade, N. Aghanim, Y. Akrami, M.I.R. Alves et al., *Planck 2015 results. I. Overview of products and scientific results*, *A&A* **594** (2016) A1 [[1502.01582](#)].
- [174] Planck Collaboration, N. Aghanim, Y. Akrami, F. Arroja, M. Ashdown, J. Aumont et al., *Planck 2018 results. I. Overview and the cosmological legacy of Planck*, *A&A* **641** (2020) A1 [[1807.06205](#)].
- [175] S.J. Turnbull, M.J. Hudson, H.A. Feldman, M. Hicken, R.P. Kirshner and R. Watkins, *Cosmic flows in the nearby universe from Type Ia supernovae*, *MNRAS* **420** (2012) 447 [[1111.0631](#)].
- [176] M. Feix, E. Branchini and A. Nusser, *Speed from light: growth rate and bulk flow at  $z \sim 0.1$  from improved SDSS DR13 photometry*, *MNRAS* **468** (2017) 1420 [[1612.07809](#)].
- [177] R. Watkins, T. Allen, C.J. Bradford, A. Ramon, A. Walker, H.A. Feldman et al., *Analysing the large-scale bulk flow using cosmicflows4: increasing tension with the standard cosmological model*, *MNRAS* **524** (2023) 1885 [[2302.02028](#)].
- [178] A. Merloni, P. Predehl, W. Becker, H. Böhringer, T. Boller, H. Brunner et al., *eROSITA Science Book: Mapping the Structure of the Energetic Universe*, *arXiv e-prints* (2012) arXiv:1209.3114 [[1209.3114](#)].
- [179] K. Migkas, D. Kox, G. Schellenberger, A. Veronica, F. Pacaud, T.H. Reiprich et al., *The SRG/eROSITA All-Sky Survey. SRG/eROSITA cross-calibration with Chandra and XMM-Newton using galaxy cluster gas temperatures*, *A&A* **688** (2024) A107 [[2401.17297](#)].
- [180] M.E. Ramos-Ceja, L. Fiorino, E. Bulbul, V. Ghirardini, N. Clerc, A. Liu et al., *The SRG/eROSITA all-sky survey: X-ray scaling relations of galaxy groups and clusters in the western Galactic hemisphere*, *arXiv e-prints* (2025) arXiv:2511.14356 [[2511.14356](#)].
- [181] S. Zelmer, E. Artis, E. Bulbul, S. Grandis, V. Ghirardini, A. von der Linden et al., *The SRG/eROSITA All-Sky Survey: Constraints on ultralight axion dark matter through galaxy cluster number counts*, *A&A* **704** (2025) A346 [[2502.03353](#)].